Catalysis Letters
https://doi.org/10.1007/s10562-020-03216-w

A Novel Magnetic Immobilized Para-Aminobenzoic Acid-Cu(II) Complex: A Green, Efficient and Reusable Catalyst for Aldol Condensation Reactions in Green Media

Zohreh Esam[1,2] · Malihe Akhavan[1] · Ahmadreza Bekhradnia[1,3] · Masoud Mohammadi[4] · Saeed Tourani[1]

Received: 28 February 2020 / Accepted: 4 April 2020

Abstract

In this the study a novel, efficient and recoverable heterogeneous nanocatalyst with regards to green chemistry purpose was approached. The structure of the newly synthesized heterogeneous magnetic nanocatalyst with enhanced and improved catalytic efficiency were determined by various instrumental techniques, including SEM, VSM, TGA, XRD, UV–VIS FT-IR and EDXA. The results, showed that the synthesized nanoparticles are superparamagnetic with a size range of 10–20 nm. Then the catalytic activity and efficient performance of Fe_3O_4@PABA-Cu(II) MNPs were analyzed toward the synthesis of novel 5-arylidenthiazolidine-2,4-diones and 5-arylidene-2-imidazolidine-2,4-dione derivatives via aldol condensation reactions between a variety of (hetero) aromatic aldehydes and hydantoin or thiazolidine-2,4-dione multifunctional privileged scaffolds under reflux condensations in ethanol as a benign solvent. Nontoxic nature and environment-friendly properties of the catalyst, simple workup, short time of reaction, easy separation of the catalyst from products, efficiency, and excellent yields are beneficial aspects of this method.

Graphic Abstract

It is the first report of aldol synthesis of new 5-arylidenthiazolidine-2,4-dione, and 5-arylidene-imidazolidine-2,4-dione derivatives using a reusable copper-PABA complex supported on Fe_3O_4 MNPs (Fe_3O_4@PABA-Cu(II)) catalyst in Green media.

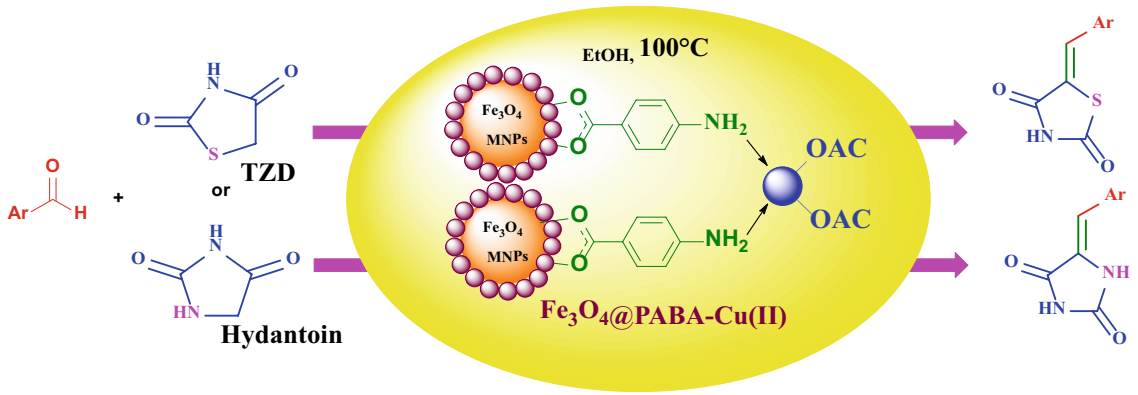

Keywords Aldol condensation · Fe_3O_4@PABA-Cu(II) · Magnetic nanocatalyst · 5-Arylidenthiazolidine-2,4-diones · 5-Arylidene-2-imidazolidine-2,4-dione

Electronic supplementary material The online version of this article (https://doi.org/10.1007/s10562-020-03216-w) contains supplementary material, which is available to authorized users.

✉ Malihe Akhavan
akhavannn@yahoo.com

Extended author information available on the last page of the article

1 Introduction

In recent years, catalytic reactions and various metal catalysts, such as nickel, cobalt, palladium, and, top of all, copper as a cheap source of the catalytic species, have received

Published online: 08 May 2020

considerable industrial applications and increasing attention in fundamental (basic) researches [1–6]. Despite all the advantages these catalysts have, especially good results, isolation and recovery of these tiny particles from the reaction mixture are painstaking since they cannot be efficiently filtered out of the reaction medium [7–10]. Thus, metal pollution of products is one of our major problems with this condition [2, 3, 11–13].The immobilization of metal catalysts on solid supports, such as magnetic nanoparticles (MNPs) because of their super paramagnetic properties, is an extremely useful way to overcome problems mentioned above [7, 8, 14–23]. The particles become magnetized through exposure to a simple external magnetic field and can be collected from the reaction mixture easily; however, without an external magnet, they exhibit any residual magnetic interactions and can be well-dispersed in the reaction mixture [24–32].In order to prevent the magnetostatic interactions between these supermagnetic nanoparticles and their aggregation due to the anisotropic dipole attraction and subsequent deactivation of a catalyst via dimerization, the surface of the MNPs is usually modified with a suitable coating agent such as silica layer, different kinds of amine-containing organic compounds. or vitamins [9, 29, 33–38]. These coating layers also work as a connecting bridge between MNPs (Fe_3O_4: as core) and our metal catalysts (Cu(II): as shell) [1, 3, 11, 39, 40].Therefore, the generation of heterogeneous metal catalysts using coated MNPs has found wide applications because of their easy availability, high surface area, and Consequently, higher catalyst loading capacity, easy isolation, minimum metal contamination and reusability which is important from both an environmental and an economic viewpoint [11, 41]. Hydantoin and Thiazolidine (TZD) are multifunctional privileged scaffolds in medicinal chemistry which represent core structures of drugs and various kinds of medicinal and biologically active agents which are considered as important classes of heterocyclic useful compounds with a broad range of therapeutic effects and pharmacological activities, leading to successful clinically approved antidiabetic drugs such as rosiglitazone and pioglitazone [42, 43]. As a consequence of the importance of hydantoin and TZD structural and functional scaffolds, numerous strategies for the synthesis of their derivatives, especially via aldol condensation reactions were already developed using extensive and different kinds of catalysts such as alum [44], ionic liquids [45], glycine [46], sodium carbonate [47], piperidinium acetate, and piperidine [48]. Some of these methodologies involve strong base conditions, low yields, long reaction times, and tedious work-up procedures They also leave toxic residues, require special apparatus, use environmentally unfavourable solvents, and require excess amounts of catalysts [45, 46].

However, over the last decade, more efforts have been taken to design environmentally benign recyclable heterogeneous catalyst which has the ability to work for the target reaction, economically feasible and produce minimum waste. In this regard, the application of graphene based materials as metal free carbocatalyst have gained significant attention in recent past in many organic transformations [16, 17]. The presence of structural defects and various oxygen functionalities such as, epoxy, hydroxyl and carboxyl groups on the surface of graphene have immensely contributed to the mild acidic as well as oxidative properties of these materials [18]. Such type of graphene like materials is typically referred to as highly reduced graphene oxide (HRG), which are often functionalize with various substances including solid acids like phosphomolybdic acid via strong electrostatic interaction to enhance their physicochemical properties and catalytic potential [19].

Recently, copper(II) has been developed as a successful catalyst for aldolization with high yields. Nevertheless, one of the most important issue for the synthetic organic chemist is minimizing waste and maximizing sustainability in order to achieve green chemistry goals. However, over the last decade, more efforts have been taken to design environmentally benign recyclable heterogeneous catalyst which has the ability to work for the target reaction, economically feasible and produce minimum waste. In this regard, the application of Fe_3O_4@PABA-Cu(II)nanocatalyst have investigated in aldol condensation of various aromatic and heteroaromatic aldehydes with hydantoin or thiazolidine (TZD) under Knoevenagel transformations conditions. To the best of our knowledge, it is the first report of utilization of heterogenized copper(II) catalysts for the one-pot preparation of 5-arylidenthiazolidine-2,4-diones and 5-arylidene-imidazolidine-2,4-dione under green media.

In this study, we used Para-aminobenzoic acid (PABA), a well-known antioxidant and water-soluble vitamin of B-group vitamins and precursor in the synthesis of folic acid, purines, thymine and also Coenzyme Q with a proper and efficient MNPs coating property as a safe bi-functional bridge to immobilize copper particles on Fe_3O_4 MNPs [49]. PABA, as one of the widely used building blocks in design and development of drugs, is frequently found as a structural and functional moiety in pharmacologically active agents [50]. Through surface modification of non-toxic MNPs, such as iron oxide Fe_3O_4 MNPs with this simple vitamin as a very stable, safe and environment-friendly organic compound which has a strong affinity to Fe_3O_4 surface hydroxyl groups via its COOH moiety and then loading copper via its amine functional group to enhance the catalytic activity of Fe_3O_4@PABA, we developed a novel, highly efficient, stable, safe and low-cost magnetically recoverable nanocatalyst Fe_3O_4@PABA-Cu(II) which can reduce

the problems associated with using mineral catalysts in aldol condensation reactions and can be removed and separated from the liquid medium of the reaction mixture easily using a very simple external magnet after the reaction went to completion. In this procedure, we found that Fe_3O_4@PABA also exhibit notable catalytic activity.

Our newly designed heterogeneous magnetic nanocatalyst Fe_3O_4@PABA-Cu(II) presents an excellent catalytic activity in Aldol condensation reactions. This efficient novel nanocatalyst which showed good performance in the above-mentioned reactions under green conditions, is recoverable easily.

2 Experimental

2.1 Synthesis of Fe_3O_4@PABA-Cu(II) MNPs

The Fe_3O_4 magnetic nanoparticles were prepared by the coprecipitation technique as it was previously reported [51]. In order to prepare Fe_3O_4@PABA, 1 g of the prepared Fe_3O_4 MNPs was dispersed in 100 mL deionized water by sonication for 30 min. in the next step, PABA was added at a concentration of 50 mg/mL to the reaction mixture, which was stirred for 8 h. Thereafter, the obtained MNPs were washed with deionized water few times to eliminate excess PABA then, Fe_3O_4@PABA MNPs were collected by magnet, and eventually dried under vacuum at 70 ºC for 12 h. Finally, Fe_3O_4@PABA-Cu(II) was prepared by the immobilization of Cu $(OAc)_2$ (0.29 g, 1.5 mmol) with 1 g of Fe_3O_4@PABA in ethanol (50 mL) under reflux conditions for 8 h. The final Fe_3O_4@PABA-Cu(II) MNPs was washed with methanol and dried under vacuum at 70 °C for 6 h.

2.2 General Procedure for the Aldol Condensation Reaction

Fe_3O_4@PABA-Cu(II) (0.05 g) was added to a mixture of various aldehydes (1 mmol), with hydantoin or TZD (1 mmol), in Ethanol (10 mL), and this mixture was refluxed for the times reported in Table 2. the progress of the reaction monitored by TLC, after completion of the reaction the mixture was diluted with ethanol and the catalyst was easily separated from the reaction mixture by an external magnet, washed with hot ethanol, dried and reused for a consecutive run under the same reaction conditions. Afterwards, the reaction mixture was cooled to room temperature and the crude product obtained was collected by filtration and washed with cold ethanol to give the pure solid.

2.3 Selected Spectral Data

2.3.1 (Z)-5-(2-oxo-2-(p-tolyl)ethylidene) thiazolidine-2,4-dione (1a)

IR (KBr, v_{max}, cm^{-1}): 3458 (N–H) 1745, 1699 (N–C=O), 600–800 (C–S), 3126 (Ar–CH) cm^{-1}; ^{1}H-NMR (400 MHz, DMSO-d_6): δ (ppm) 2.48 (s, 3H, CH_3), 7.15(d, $J = 8.8$ Hz, 2H, ArH), 7.85(d, $J = 8.8$ Hz, 2H, ArH), 6.98 (s, 1H, = CHAr), 10.82 (brs, 1H, NH);^{13}C-NMR (100 MHz, DMSO-d_6): ppm 22.46, 128.83, 129.44, 134.47, 144.75, 142.43, 148.98, 185.42, 168.66, 187.17, 189.61.MS: (m/z, %) 248 (M^+, 17), 276 (17), 204 (14), 190 (43), 132(21), 118 (100), 91.0 (63), 77.0 (15), 65.0 (%35), 51.0(30); Elemental anal. (%), calced for $C_{12}H_9NO_3S$:C, 66.64; H, 3.41; N, 5.83; found: C, 58.03; H, 3.67; N, 5.66.

2.3.2 (Z)-5-(2-oxo-2-(p-tolyl)ethylidene) imidazolidine-2,4-dione (1b)

IR (KBr, v_{max}, cm^{-1}): 3193(N–H), 1735 (N–C=O), 3015 (Ar–CH) cm^{-1}; ^{1}H-NMR (400 MHz, DMSO-d_6): δ (ppm) 2.75 (s, 3H, CH_3), 7.34 (d, $J = 8.8$ Hz, 2H, ArH), 7.76 (d, $J = 8.8$ Hz, 2H, ArH), 6.89 (s, 1H, =CHAr), 10.89 (bs, 1H, NH) 7.85 (1H, NH); ^{13}C-NMR (100 MHz, DMSO-d_6): ppm 23.26, 129.99, 130.44, 138.57,146.55, 145.12, 148.20, 186.44,188.59, 190.17,195.61. MS: (m/z, %) 230.01 (M^+, 17), 222 (25), 167.0 (37), 143 (79), 132 (100), 102.0 (35), 119 (18), 71.0 (27), Elemental anal. (%), calced for $C_{12}H_{10}N_2O_2$: C, 62.61; H, 4.38; N, 12.17; found: C, 63.73; H, 4.45; N, 11.32.

2.3.3 (Z)-5-(2-(4-bromophenyl)-2-oxoethylidene) thiazolidine-2,4-dione (2a)

IR (KBr, v_{max}, cm^{-1}): 3044 (NH), 1684 (N–C=O), 1582 (C=C), 1465 (C=N), 849 (C–Br), 1038 (C–N), 2829 (CH–Ar) cm^{-1}; ^{1}H-NMR (400 MHz, DMSO-d_6): δ (ppm) 6.99 (s, 1H, =CH), 7.23 (d, $J = 8.8$ Hz, 2H, ArH), 8.21 (d, $J = 8.8$ Hz, 2H, ArH), 10.7 (brs, 1H, NH); ^{13}C NMR (100 MHz, DMSO-d_6): ppm 128.67, 133.14, 136.87, 140.51, 145.44, 149.71, 185.01, 168.95, 187.01, 189.71; MS: (m/z, %) 311.2. (M^+, 7), 281.1 (6), 255.9 (3), 203 (10), 188 (14), 155.9 (57), 138.9 (100), 110.9 (48), 91 (16), 75 (35), 51 (15); Elemental anal. (%), calced for $C_{11}H_6BrNO_3S$:C, 42.33; H, 1.94; N, 4.49; found: C, 42.09; H, 2.21; N, 6.07.

2.3.4 (Z)-5-(2-(4-bromophenyl)-2-oxoethylidene) imidazolidine-2,4-dione (2b)

IR (KBr, v_{max}, cm^{-1}): 3420 (NH), 1741 (N–C=O), 1189(N–C=S), 1581 (C=C), 841 (C–Br), 2829 (CH–Ar) cm^{-1}; ^{1}H NMR (400 MHz, DMSO-d_6): δ (ppm): 6.97 (s, 1H, =CH), 7. 93 (d, $J = 8.8$ Hz, 2H, ArH), 8.17(d, $J = 8.8$ Hz, 2H, ArH) 7.90 (1H, NH), 12.90 (brs, 1H, NH); ^{13}C-NMR (100 MHz, DMSO-d_6): ppm 131.35, 129.54, 134.57, 138.60, 144.44, 148.48, 181.51, 188.56, 189.97, 198.64; MS: (m/z, %) 295. (M^+, 10); 279 (7), 207 (60), 188 (32), 182 (22), 171 (40), 154 (37), 143 (75), 110 (27), 85 (57),55(100); Elemental anal. (%), calced for $C_{11}H_7BrN_2O_3$: C, 44.77; H, 2.39; N, 9.49; found: C, 40.36; H, 1.73; N, 4.24.

2.3.5 (Z)-5-(2-(4-methoxyphenyl)-2-oxoethylidene) thiazolidine-2,4-dione (3a)

IR (KBr, v_{max}, cm^{-1}): 3438 (N–H), 1682 (C=O stretching), 3025 (Ar–CH),1542 cm^{-1}; ^{1}H NMR (DMSO-d_6): δ = 3.56 (s, 3H, OCH_3), 6.70 (s, 1H CH=), 7.37–7.38 (d, $J = 8.8$ Hz, 2H, ArH), 8.12–8.13 (d, $J = 8.8$ Hz, 2H, ArH), 12.66 (brs, 1H, NH); ^{13}C NMR (DMSO-d_6): ppm 58.10, 103.48, 122.66, 130.83, 131.41, 141.94, 149.36, 170.31, 171.31, 180.04, 182.03; MS: (m/z, %) 263 (M^+, 11), 248 (%8),235.9 (9), 220.01 (13), 206.0 (44), 191.0 (9), 177.0 (14), 162.0 (8), 140.1 (16), 134 (100), 121.0 (14), 109 (48), 91.0 (35), 77.0 (35), 51.0 (29), (%) Elemental anal. (%), calced for $C_{12}H_9NO_4S$:C, 54.75; H, 3.45; N, 5.32; found: C, 54.15; H, 2.95; N, 6.12.

2.3.6 (Z)-5-(2-(4-methoxyphenyl)-2-oxoethylidene) imidazolidine-2,4-dione (3b)

IR (KBr, v_{max}, cm^{-1}):3433(N–H), 1701 (C=O), 1643 (C=C), 1189 cm^{-1};^{1}H NMR (DMSO-d_6, 400 MHz): δ = 3.83 (s, 3H, OCH_3),), 6.95 (s, 1H, CH=), 6.93 (d, $J = 8.8$ Hz, 2H, ArH), 7.31 (d, $J = 8.8$ Hz, 2H, ArH), 7.70 (1H, NH); 11.71 (brs, 1H, NH);^{13}C NMR (DMSO-d_6): ppm 56.92, 103.26, 125.66, 128.13, 136.68, 144.38, 151.08, 168.44, 187.58, 187.71, 189.8; MS: (m/z, %) 246 (M^+, 11), 248 (4), 207 (53), 188.9 (28), 167 (33), 143 (80), 162 (6), 125 (28), 111 (24),85 (55), 71.1 (66), 57.01 (100); Elemental anal. (%), calced for $C_{12}H_{10}NO_4$: C, 58.54; H, 4.09; N, 11.38; found: C, 59.06; H, 3.25; N, 10.29.

2.3.7 (Z)-5-((1-methyl-1H-indol-2-yl)methylene) thiazolidine-2,4-dione (4a)

IR (KBr): νmax 3435 (N–H), 1729, 1685 (N–C=O), 600–800(C-S), 3132 (Ar–CH) cm^{-1}; ^{1}H-NMR (400 MHz, DMSO-d_6): δ (ppm) 12.60 (s, broad, 1H), 7.85 (s.1H), 7.68 (dd, 1H), 7.55 (dd, 1H), 7.38 (dt, 1H), 7.11 (dt, 1H) 7.04 (s, 1H, CH=), 3.88 (s,3H); ^{13}C-NMR (100 MHz, DMSO-d_6): 34.17,101.09, 111.1, 119.23, 120.12, 121.19, 122.20, 125.80, 131.58, 135.10, 140.05, 166.36, 168.19; MS: (m/z, %), 259 m/z (M^+, 11), 232 (4), 206 (53), 187 (34), 182.9 (27), 143 (80), 162 (6), 127 (28), 114 (24),76 (55), 74.1 (66), 59.01 (100); Elemental anal. (%), calced for $C_{13}H_{10}N_2O_2S$:C, 60.54; H, 3.90; N, 10.85; found: C, 59.06; H, 3.25; N, 10.29.

2.3.8 (Z)-5-((1-methyl-1H-indol-2-yl)methylene) imidazolidine-2,4-dione (4b)

IR (KBr): νmax3430 (N–H), 1765 (N–C=O), 1699 (N–C=O) cm^{-1}; ^{1}H-NMR (400 MHz, DMSO-d_6): δ (ppm) 13.34 (brs, 1H, NH), 9.84 (s, 1H, NH) 7.12 (s.1H), 6.89–692 (m,1H), 7.27–7.28 (m, 1 H), 7.29–7.35 (m, 1H), 7.48–7.51(m, 1H), 6.97 (s, 1H, CH=), 3.18 (s, 3H); ^{13}C-NMR (100 MHz, DMSO-d_6): 34.16, 106.72, 111.27, 120.65, 122.66, 126.17, 127.17, 130.83, 131.41, 141.94, 150,61, 155.44, 163.16; MS: (m/z, %), 242 m/z (M^+, 27), 215 (43), 198 (44), 143 (75), 170 (36), 130 (48), 111 (43),76 (55), 71.1 (100); Elemental anal. (%), calced for $C_{13}H_{11}N_3O_2$: C, 64.72; H, 4.60; N, 17.42; found: C, 63.06; H, 3.25; N, 16.29.

2.3.9 (Z)-5-((5-nitrothiophen-2-yl)methylene) thiazolidine-2,4-dione (5a)

IR (KBr): νmax 3438 (N–H), 1683 (N–C=O), 3054 (Ar–CH) cm^{-1}; ^{1}H-NMR (400 MHz, DMSO-d_6): δ (ppm), 13.08 (brs, 1H, NH), 8.05–8.06 (dd, 1H), 8.36–8.37 (s.1H, CH=), 7.56 (dd, 1H); ^{13}C-NMR (100 MHz, DMSO-d_6): 123.22, 130.09, 140.96, 144.37, 144.38, 145.37, 155.36, 167.32, 168.32; MS: (m/z, %), 255 m/z (M^+, 27), 212 (51), 184 (54), 152 (45), 180 (26), 127 (68), 102 (43), 71.1 (100); Elemental anal. (%), calced for $C_8H_4N_2O_4S_2$: C, 37.50; H, 1.57; N, 10.93; found: C, 36.06; H, 1.05; N, 11.29.

2.3.10 (Z)-5-((5-nitrothiophen-2-yl)methylene) imidazolidine-2,4-dione (5b)

IR (KBr): νmax 3445(N–H), 1722 (N–C=O), 3050 (Ar–CH) cm^{-1}; ^{1}H-NMR (400 MHz, DMSO-d_6): δ (ppm): 12.91 (brs, 1H, NH), 10.68 (s, 1H, NH), 7.14–7.16 (dd, 1H), 7.91–7.92 (dd.1H), 6.97 (s,1H, CH=); ^{13}C-NMR (100 MHz, DMSO-d_6): 114.49, 130.09, 132.87, 140.95, 148.12, 155.36, 162.79, 168.07; MS: (m/z, %), 239 m/z (M^+, 46), 195 (54), 168 (46), 136 (35), 127 (68),111(39), 102 (25), 71.1 (100); Elemental anal. (%), calced for $C_8H_5N_3O_4S$:C, 40.17; H, 2.11; N, 17.57; found: C, 39.06; H, 1.15; N, 16.29.

2.3.11 (Z)-5-((5-hydroxyfuran-2-yl)methylene) thiazolidine-2,4-dione (6a)

IR (KBr): νmax: 3440 (NH), 1722 (N–C=O), 1583 (C=C), 2994 (CH–Ar) cm^{-1}; ^{1}H-NMR (400 MHz, DMSO-d_6): δ (ppm) 12.41 (brs, 1H, NH), 10.52 (s, 1H, OH), 6.96 (s, 1H, CH=), 7.35–7.36 (dd.1H), 6.48–7.49 (dd, 1H); ^{13}C-NMR (100 MHz, DMSO-d_6): 113.42, 114.61, 122.80, 131.10, 133.66, 141.82, 162.71, 166.82; MS: (m/z, %), 210 m/z (M^+, 51), 193 (34), 168 (41), 136 (21), 127 (68),114(31), 83(54), 71.1 (100); Elemental anal. (%), calced for $C_8H_5NO_4S$:C, 45.50; H, 2.39; N, 6.63; found: C, 44.06; H, 2.15; N, 5.29.

2.3.12 (Z)-5-((5-hydroxyfuran-2-yl)methylene) imidazolidine-2,4-dione (6b)

IR (KBr): νmax 3383 (NH), 1752 (N–C=O), 1594 (C=C) cm^{-1}; ^{1}H-NMR (400 MHz, DMSO-d_6): δ (ppm): 12.48 (brs, 1H, NH), 10.73 (brs, 1H, NH), 10.51 (s, 1H, OH), 6.94 (s, 1H, CH=), 6.72–6.73 (dd.1H), 7.04–7.05 (dd, 1H); ^{13}C-NMR (100 MHz, DMSO-d_6): ppm 110.46, 113.42, 122.80, 131.10, 141.82, 159.09, 162.71, 169.56; MS: (m/z, %), 194 m/z (M^+, 51), 177 (26), 179 (21), 152 (18), 136 (61),111 (23), 83(46), 71.1 (100); Elemental anal. (%), calced for $C_8H_5N_2O_4$: C, 49.49; H, 3.12; N, 4.43; found: C, 48.06; H, 2.15; N, 5.02.

2.3.13 (Z)-5-((3-hydroxy-1H-pyrrol-1-yl) methylene) thiazolidine-2,4-dione (7a)

IR (KBr): νmax 3415 (N–H), 1735 (N–C=O), 3038 (Ar–CH), cm^{-1}; ^{1}H-NMR (400 MHz, DMSO-d_6): δ (ppm): 12.58 (brs, 1H, NH), 10.47 (s, 1H, OH), 7.49 (s, 1H), 7.28–7.31 (m.1H), 7.35–7.36 (d, 1H), 6.90 (s, 1H, CH=);^{13}C-NMR (100 MHz, DMSO-d_6): 105.48, 113.42, 119.19, 122.80, 133.66, 162.71,168.32; MS: (m/z, %), 210 m/z (M^+, 61), 193 (56), 169 (22), 135 (100), 126 (42), 82(65); Elemental anal. (%), calced for $C_8H_6N_2O_3S$:C, 45.71; H, 2.88; N, 13.33; found: C, 45.06; H, 2.10; N, 12.02: MS: (m/z, %) 194 (M^+, 176 (100), 111 (29), 135 (20), 82 (27), 86 (2), 63 (11); Elemental anal. (%), calced for $C_8H_7N_3O_3$: C, 49.74; H, 3.65; N, 21.75; found C, 48.25, H 2.53, N, 20.07.

2.3.14 (Z)-5-((3-hydroxy-1H-pyrrol-1-yl)methylene) imidazolidine-2,4-dione (7b)

IR (KBr): νmax 3424 (N–H), 1754 (N–C=O), 3064 (Ar–CH), cm^{-1}; ^{1}H-NMR (400 MHz, DMSO-d_6): δ (ppm): 12.44 (brs, 1H, NH); 10.96 (brs, 1H, NH),10.29 (s, 1H, OH), 7.82 (s, 1H, CH=), 7.98 (dd, 1H), 7.38–7.41 (dd, 1H), 7.56–7.58 (s, 1H), ^{13}C-NMR (100 MHz, DMSO-d_6): ppm 108.47, 111.46, 114.49, 123.09, 123.22, 128.17, 167.82, 169.56; MS: (m/z, %) 193 (M^+, 14), 176 (18), 151 (69), 135 (40), 111 (100), 104 (26), 82 (50), 58.1 (6); Elemental anal. (%), calced for $C_8H_7N_3O_3$: C, 94.74; H, 3.65; N, 21.75; found: C, 93.67; H, 2.04; N, 20.26.

2.3.15 (Z)-5-((2-methylpyridin-3-yl)methylene) thiazolidine-2,4-dione (8a)

IR (KBr): νmax 3438 (N–H), 1754 (N–C=O) cm^{-1}; ^{1}H-NMR (400 MHz, DMSO-d_6): δ (ppm): 11.31 (brs, 1H, NH), 8.57 (dd, 1H), 6.65 (s, 1H, CH=), 7.22–7.25 (m, 1H), 7.37–7.39 (m, 1H) 8.13–8.17(m, 1H); 2.94 (s, 3H),^{13}C-NMR (100 MHz, DMSO-d_6): ppm 32.66, 122.78, 123.92, 131.10, 133.65, 141.81, 150.61, 162.71, 167.82, 169.06; MS: (m/z, %) 220. (M^+, 42), 205.1 (23), 190 (23), 160 (7), 149 (42), 127.5 (9), 118.5 (100), 92.0 (65), Elemental anal. (%), Calcd for $C_{10}H_8N_2O_2S$:C, 54.53, H, 3.66; N, 12.72. found: C, 53.88, H, 2.61; N, 11.73.

2.3.16 (Z)-5-((2-methylpyridin-3-yl)methylene) imidazolidine-2,4-dione (8b)

IR (KBr): νmax 3123 (N–H), 1727 (N–C=O), 2800 (Ar–CH) cm^{-1}; ^{1}H-NMR (400 MHz, DMSO- d_6): δ (ppm): 11.19 (brs, 1H, NH), 9.92 (1H, NH) 6.65 (s, 1H, CH=), 7.37–7.39 (m, 1H), 7.75–7.76 (d.1H), 8.13–8.17 (m, 1H); 3.12 (s, 3H),^{13}C-NMR (100 MHz, DMSO-d_6): ppm 33.41, 123.09, 123.22, 130.09, 132.87, 140.95, 155.36, 162.79, 168.32, 169.56; MS: (m/z, %) 203.1 (M^+, 32), 188 (32), 175 (8), 161 (10), 111 (100), 92 (69), 71.1 (11), Elemental anal. (%), Anal. Calced. for $C_{10}H_9N_3O_2$: C, 59.11; H, 4.46; N, 20.68. found: C, 58.01; H, 3.83; N, 19.15.

2.3.17 (Z)-5-(4-hydroxy-3-methoxybenzylidene) thiazolidine-2,4-dione (9a)

IR (KBr): νmax 3042(N–H), 1638(N–C=S), 1730 (N–C=O), 1479 (C=C), 2674 (Ar–CH) cm^{-1}; ^{1}H NMR (400 MHz, $CDCl_3$): δ (ppm) 12.47 (s, 1H),0 9.96 (s, 1H), 7.71 (s, 1H, CH=), 0 7.17 (d, J = 1.83 Hz, 1H), 07.08 (dd, J = 8.04 and 1.83 Hz, 1H), 0 6.93 (d, J = 8.04 Hz, 1H), 0 3.86 (s, 3H) ^{13}C-NMR (100 MHz, $CDCl_3$): δ (ppm) 168.5, 168.2, 149.6, 148.3, 133.3, 125.3, 124.7, 119.6, 115.7, 113.2, 55.2; MS: (m/z, %) 251. (M^+, 32), 276.1 (23), 223 (13), 208 (17), 182 (50), 152 (10), 127.5 (19), 124.5 (100), 98.0 (65), 71 (43) Elemental anal. (%), Calcd for $C_{11}H_9NO_4S$:C, 52.58; H, 3.61; N, 5.57. found: C, 51.88; H, 2.41; N, 5.03.

2.3.18 (Z)-5-(4-hydroxy-3-methoxybenzylidene) imidazolidine-2,4-dione (9b)

IR (KBr): νmax 3223 (N–H), 1739, 1698 (N–C=O), 1580 (C=C), 2094 (Ar–CH) cm^{-1}; ^{1}H-NMR (400 MHz, $CDCl_3$): δ (ppm 11.11 (s, 1H), 10.40 (s, 1H), 9.42 (s, 1H), 7.09 (d, 1H, J = 1.5 Hz), 7.06 (dd, 1H, J = 1.5, 8.5 Hz), 6.78 (d, 1H, J = 8.5 Hz), 6.95 (s, 1H,CH=), 3.82 (s, 3H); ^{13}C-NMR (100 MHz, CDCl3):δ (ppm) 166.3, 156.4, 148.4, 148.2, 126.1, 125.0, 124.1, 116.4, 113.8, 110.5, 56.4 MS: (m/z, %) 234. (M^+, 41), 203 (19), 191 (15), 186 (10), 163 (21), 123.5 (19), 111.5 (100), 92.0 (16), 71 (32) Elemental anal. (%), Calcd for $C_{11}H_{10}N2O_4$: C, 56.41; H, 4.30; N, 11.96. found: C, 55.88; H, 3.01; N, 10.02.

2.3.19 (Z)-5-(2, 4-dichlorobenzylidene)-thiazolidine-2,4-dione (10a)

IR (KBr, v_{max}, cm^{-1}): 3054 (N–H), 1712 (C=O), 1433(C=C) cm^{-1}; ^{1}H NMR (400 MHz, DMSO-d_6, δ ppm: 7.23 (s, 1H, Ar), 7.26 (d, J = 7.52 Hz, 1H, ArH), 7.36 (d, J = 7.51 Hz, 1H, ArH), 7.81 (s, 1H, C=CH), 12.64 (brs, 1H, N–H); ^{13}C-NMR (100 MHz, DMSO-d_6; δ ppm): 119.18, 135.58, 128.31,137.12, 127.91, 128.97, 142.12, 125., 167.20, 166.19. HRMS$^+$, calculated: 274.1233, found: 274.1073. Elemental anal. (%), calced for $C_{10}H_5$ Cl_2NO_2S:C, 43.82; H, 1.84; N, 5.11; found C, 43.61, H, 2.05, N, 5.36.

2.3.20 (Z)-5-(2,4-dichlorobenzylidene) imidazolidine-2,4-dione (10b)

IR (KBr, vmax, cm^{-1}): 3039 (NH), 2929 (CH–Ar), 1728 (C=O), 1574 (C=C), 1442 (C=N), 1047 (C–N) cm^{-1}; ^{1}H NMR (400 MHz, DMSO-d6): δppm 13.81 (brs, 1H, NH), 12.01 (brs, 1H, NH); 7.77 (s, 1H, CH=), 7.33–7.61 (m, 3H), ^{13}C NMR (100 MHz, DMSO-d6): δppm = 116.2, 125.21, 126.35, 128.44, 130.29, 131.40, 136.51, 143.24, 168.03, 193.31. MS: (m/z, %) 255. (M^+, 35), 220 (19), 212 (18), 186 (10), 144 (21), 111.5 (34), 97.0 (15), 71 (12) Elemental anal. (%), calced for $C_{10}H_6$ $Cl_2N_2O_2$:C, 46.72; H, 2.35; N, 27.58; found C, 45.65, H, 1.69, N, 26.62.

3 Results and Discussion

3.1 Catalyst Preparation

In this work, in the first step Fe_3O_4 MNPs core–shell were synthesized using co-precipitation of Fe^{3+} and Fe^{2+} ions in presence of ammonia medium 47. Then, loading of PABA on the magnetic nanoparticles through the reaction of hydroxyl functional groups on the surface of Fe_3O_4 MNPs with carboxylic acid functional group of PABA in Ethanol, formed Fe_3O_4@PABA intermediate with observable catalytic activity. Finally treating Fe_3O_4@PABA with Cu(II) and complexation was performed with an excess amount of cupric acetate solution (Copper(II) acetate) (Scheme 1).

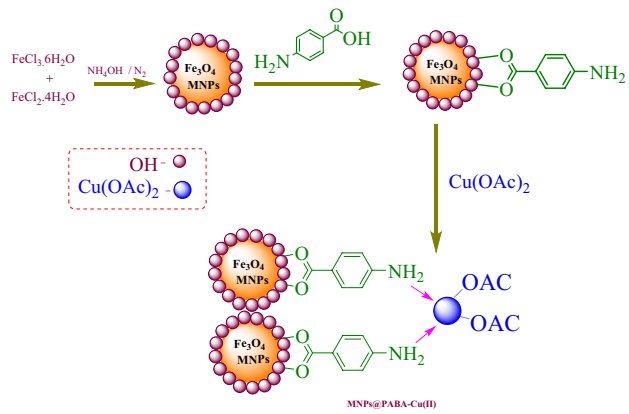

Scheme 1 Synthesis of Fe_3O_4@PABA-Cu(II) MNPs

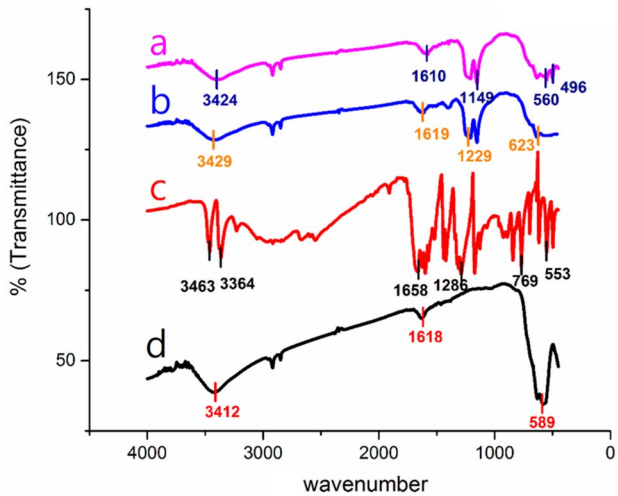

Fig. 1 FT-IR spectra: Fe_3O_4, PABA, Fe_3O_4@PABA and Fe_3O_4@PABA-Cu(II)

3.2 Catalyst Characterizations

After the successful synthesis of Fe_3O_4@PABA-Cu(II) its structure was characterized using FT-IR, XRD, EDX, AAS, TGA VSM, mapping, SEM and TEM techniques. FT-IR spectra of Fe_3O_4, PABA, Fe_3O_4@PABA and Fe_3O_4@

PABA-Cu(II) MNPs is depicted in Fig. 1, The FT-IR spectrum of Fe_3O_4 MNPs demonstrates special absorption band peaks at 1615 cm^{-1} and 585 cm^{-1} which is attributed to the twisting vibration of the H-OH band and stretching vibration of Fe–O on the surface of support, respectively (Fig. 1a). According to the Fig. 1b that is related to the FT-IR spectrum of PABA, the The characteristic signals at 3363 cm^{-1}, 3459 cm^{-1} and 1681 cm^{-1} is attributed to the C–H, O–H and C=O groups. As shown in Fig. 1c, in the FT-IR spectra of MNPs-PABA the COO–Fe, C–H, C–O and Fe–O band at 1647 cm^{-1}, 3445 cm^{-1}, 1233 cm^{-1} and 641 cm^{-1} regions, respectively confirmed the successful immobilization of PABA ligand on the surface of Fe_3O_4 support. In addition, the absorption peaks at 3363 cm^{-1} and 1624 cm^{-1} was assigned to the stretching vibration and bending vibration of the NH_2 group on aniline part of PAPA that shifted to lower wavenumber in the spectrum of Fe_3O_4@PABA-Cu(II). Also, new absorption bands at 560, 490 cm^{-1} were assigned to Cu–NH bands of the complexes [1]. These data suggested that the Fe_3O_4@PABA-Cu(II) was synthesized successfully.

According to FT-IR recovered MNPs@PABA-Cu(II) catalyst (Fig. 12c), the bands at the regions 3418 cm^{-1}, 2918 cm^{-1}, 1213 cm^{-1}, and 556 cm^{-1} approve the presence of C–H, C=O, C–O and Fe–O groups respectively). New absorption bands at 554, 504 cm^{-1} were assigned to Cu–NH bands of the complexes.

To determine the crystalline structure of PABA-Coated Fe_3O_4 (MNPs-PABA) and Fe_3O_4@PABA-Cu(II), X-ray diffraction technique was used (Fig. 1). XRD pattern of Fe_3O_4, Fe_3O_4@PABA and Fe_3O_4@PABA-Cu(II) were gathered in the region 2θ = 20º–80º. On the basis of Fig. 2, all diffraction peaks that were located at 30.2º, 35.9º, 43.3º, 53.5º, 57.4º, 63.1º, 74.5º are correspondent with (220), (311), (400), (422), (511), (440) and (533) crystalline planes of Fe_3O_4 structure, respectively (Fe_3O_4, reference Jcpds no, 82-1533). In addition, the crystalline size of Fe_3O_4@PABA-Cu(II) MNPs was estimated, using the Scherrer equation from XRD pattern data, to be 20 nm.

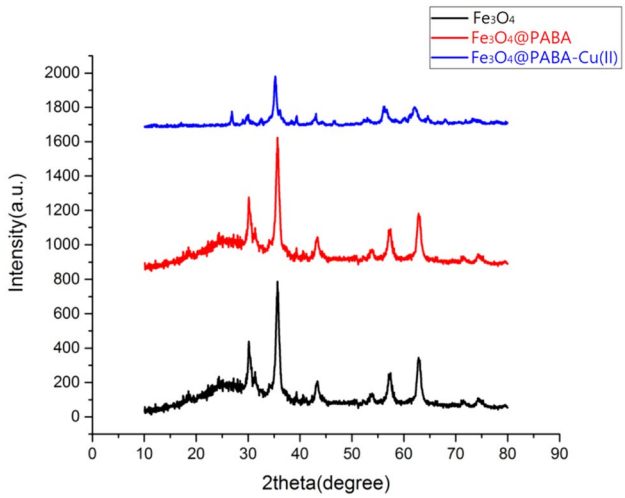

Fig. 2 XRD diffraction pattern of Fe_3O_4MNPs, Fe_3O_4@PABA and Fe_3O_4@PABA-Cu(II)

To evaluate the morphology of the Fe_3O_4@PABA and the resulting hybrid of Fe_3O_4@PABA-Cu(II), scanning electron microscopy (SEM) was used (Fig. 2). On the basis of SEM images, the catalyst has a spherical shape with a diameter 25 nm (Fig. 3).

The particle size of the synthesized Fe_3O_4@PABA-Cu(II) was evaluated by Transmission electron microscopy (Fig. 4). On the basis of TEM images, the catalyst has a spherical and nearly monodisperse shape with a diameter 30 nm.

The prepared magnetic nanocatalyst was studied using an energy dispersive spectrometer (Fig. 5). According to Fig. 5, presence of Fe, O, C, N and, Cu signals confirm that Fe_3O_4 had successfully been functionalized by PABA and then copper (II) acetate. The EDX elemental mapping from the SEM analysis clearly confirms that Fe_3O_4@PABA-Cu(II) consists of, Cu, C, O, N and Fe also absence of other elements indicate Fe_3O_4@PABA-Cu(II) have a high purity level (Fig. 6).

Thermal gravimetric analysis was applied to appraise the stability of of Fe_3O_4@PABA, Fe_3O_4@PABA-Cu(II) and bond formation between Fe_3O_4 and organic agent (PABA) (Fig. 7). The first weight loss below 100 °C can be related to the solvent desorption and surface hydroxyl groups. The second weight loss can be ascribed to the decomposition of the PABA and PABA-Cu(II) complex grafted on the surface of Fe_3O_4 support. As it can be seen from the TGA curve, the amount of organic immobilized catalytic complex was about 5.5%. Based on this weight loss, it was calculated that 0.71 mmol of PABA ligand was loaded on 1 g of Fe_3O_4 support.

The vibration sample magnetometer (VSM) of the Fe_3O_4@PABA and Fe_3O_4@PABA-Cu(II) are displayed in Fig. 8. According to Fig. 8, the saturation magnetization of the catalyst is about 45 emu/g. This magnetization value is less than the uncoated Fe_3O_4@PABA (51.3 emu/g) due to the coated shell (PABA).

The particle size distribution and zeta potential of the Fe_3O_4@PABA-Cu(II) were determined by dynamic light scattering (DLS) spectrometer in an aqueous dispersion. Particle size distribution curves showed that the average particle size of Fe_3O_4@PABA is 10 nm. The value of the zeta potential is predictive of colloidal stability. Nanoparticles with Zeta Potential values greater than + 25 mV or less than − 25 mV typically have high degrees of stability [3]. The zeta potential of the Fe_3O_4@PABA-Cu(II) in aqueous dispersion Fig. 9, were determined to be − 26.3 mV, which demonstrates high stability of Fe_3O_4@PABA-Cu(II).

The UV–Vis spectra of Fe_3O_4, PABA and Fe_3O_4@PABA-Cu(II) are demonstrated in Fig. 10. PABA

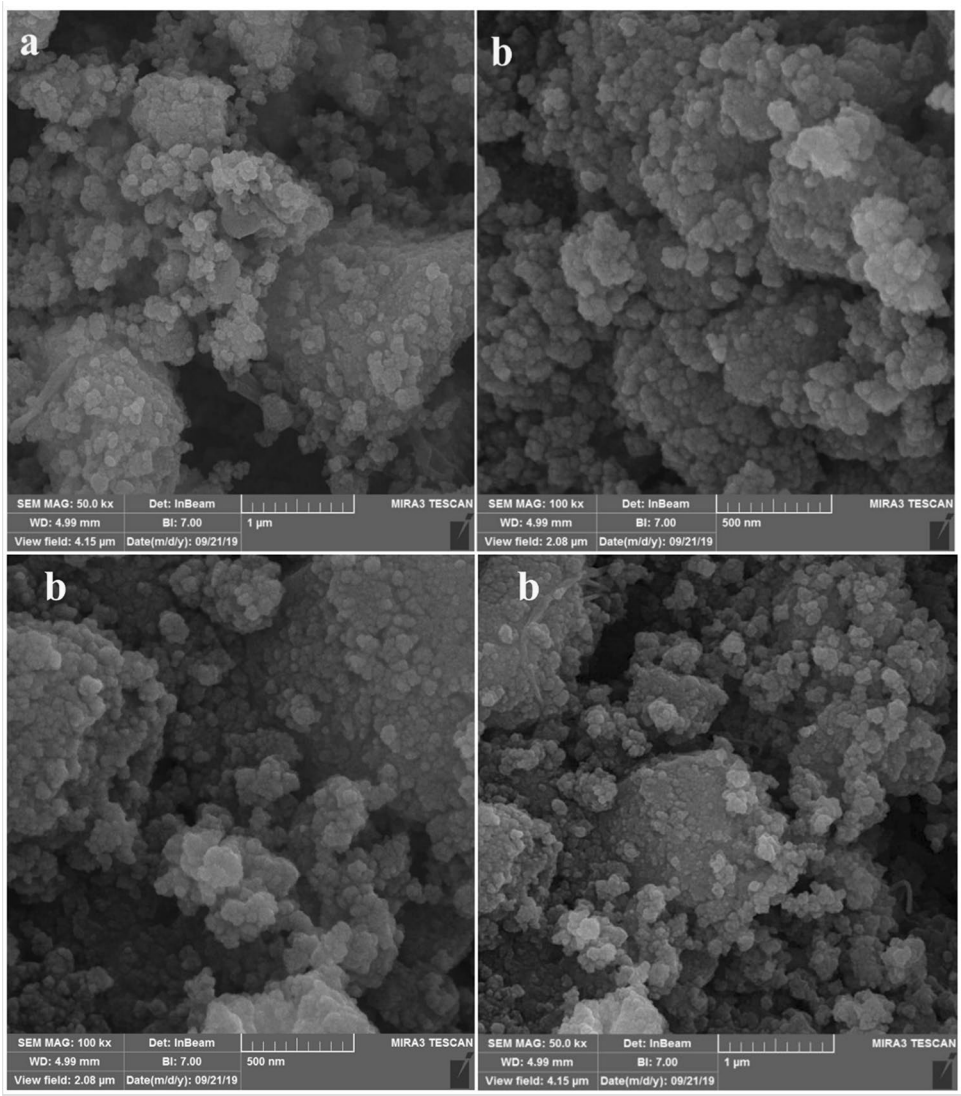

Fig. 3 SEM images of **a** Fe_3O_4@PABA and **b** Fe_3O_4@PABA-Cu(II)

represents two peaks in the UV region at 290 and 320 nm due to both conjugated (π)-bonding systems (π–π*transition) and nonbonding electron system (n–π*transition) in the compound. Fe_3O_4 nanoparticles does not show any UV–Vis characteristic absorption peaks [3], but Fe_3O_4@PABA-Cu(II), like PABA, exhibited two peaks at 290 and 320 nm [52].

The amount of residual copper in Fe_3O_4@PABA-Cu(II) was determined by atomic absorption spectroscopy (AAS) after the adsorption process using a Perkin Elmer AAnalyst 100 atomic absorption spectrophotometer with copper hollow cathode lamps and air-acetylene flame (Table 1).

After the preparation and then separation of the final catalyst (Fe_3O_4@PABA-Cu(II)) from the reaction mixture by filtration, the filtrate was subjected to quantitative elemental

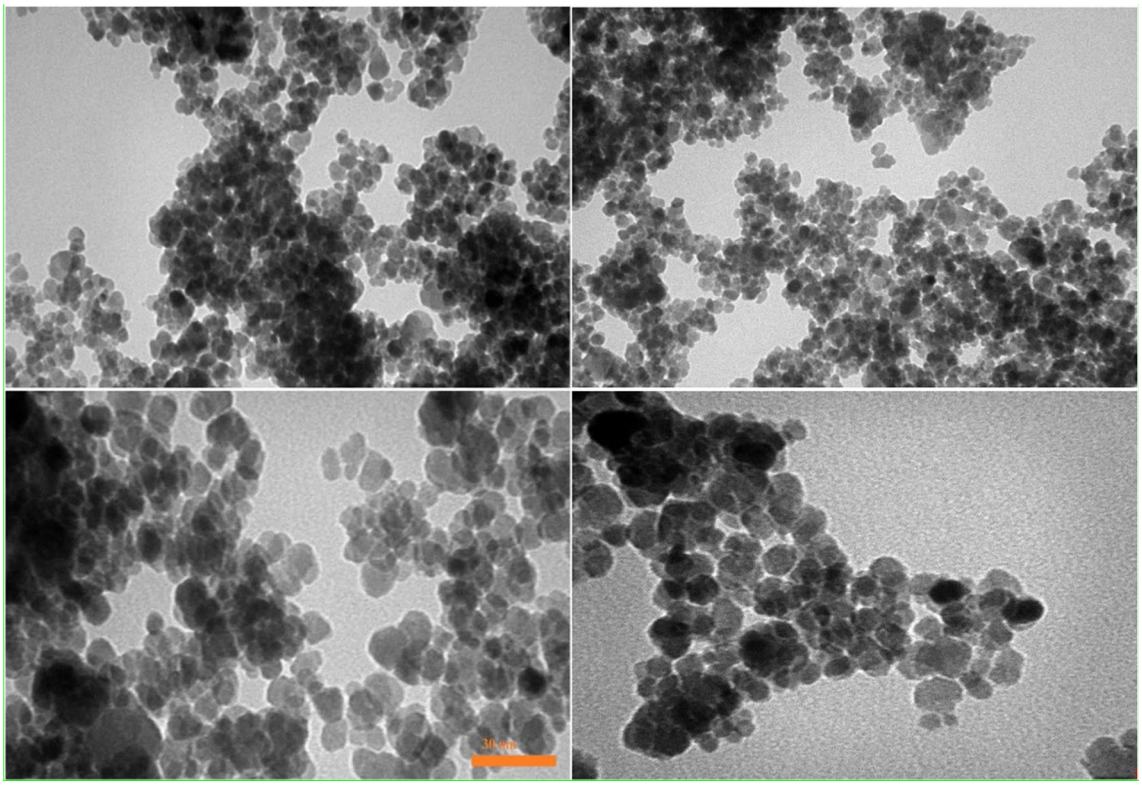

Fig. 4 TEM images of Fe_3O_4@PABA-Cu(II)

analysis. The atomic absorption was used to evaluate the concentration of Cu in the reaction filtrate (1.07 ppm) which clearly confirmed that during the reaction, Cu almost completely precipitated onto the PABA modified surface of MNPs. Prior to analysis, the calibration curve of Cu^{2+} was prepared, followed by measurements of Cu^{2+} in solutions at a wavelength of 324.8 nm. Each measurement was done in triplicate, and the average results are reported.

The Brunauer–Emmett–Teller (BET) surface areas of Fe_3O_4@PABA-Cu(II) were investigated using the nitrogen adsorption/desorption method. As is shown in Fig. 11. The BET specific surface area is 60.5 m^2/g.

3.3 Catalytic Study

After physicochemical and structural characterization of the Fe_3O_4@PABA and Fe_3O_4@PABA-Cu(II) catalysts, the generality, usefulness and, capability of these catalysts, especially the highly efficient final catalyst Fe_3O_4@PABA-Cu(II), were investigated towards aldol condensation reactions between hydantoin, TZD and diverse aldehyde derivatives. Considering the importance of hydantoin and TZD derivatives, in the present study, we want to find and demonstrate a general and practical procedure for green and facile synthesis of these compounds in high purity and yields, waste reduction, and the shorter reaction time. In order to establish the optimum reaction conditions, first, the effect of catalyst loading was examined. Thus, the condensation reaction between 2,6-Dichlorobenzaldehyde 1 (1 mmol), hydantoin 2 (1 mmol) was selected as a model reaction (Scheme 2) and the obtained results are summarized in Table 2. The best yields, time profile, and reduction of undesired side products were obtained when the reaction was carried out in the presence of 50 mg of Fe_3O_4@

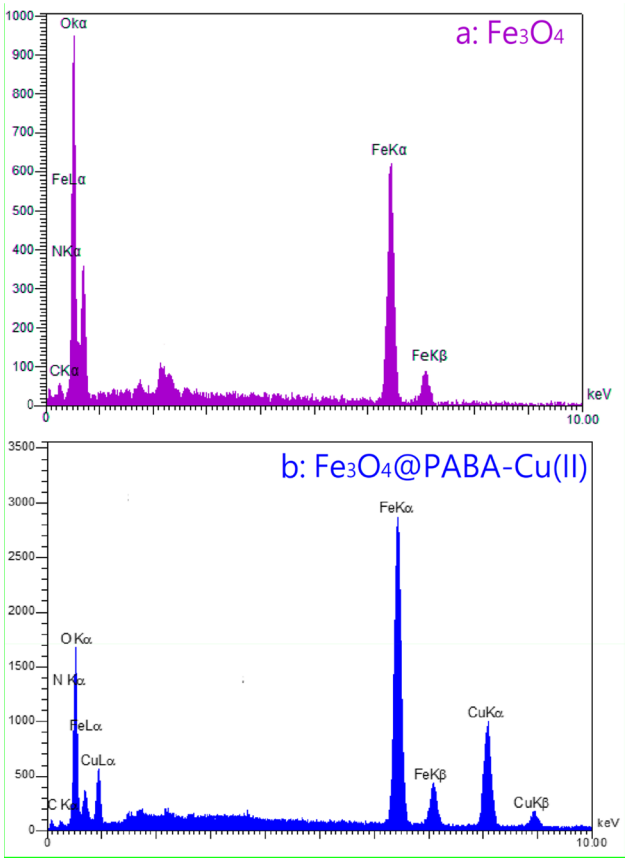

Fig. 5 Energy dispersive X-ray spectra of **a** Fe_3O_4@PABA and **b** Fe_3O_4@PABA-Cu(II)

PABA-Cu(II) under reflux conditions in Ethanol, which afforded the corresponding (Z)-5-(2,4-dichlorobenzylidene) imidazolidine-2,4-dione 10b in approximately 58 min with 98% of yield (Table 2). An increase in the quantity of Fe_3O_4@PABA-Cu(II) to more than 50 mg showed no substantial improvement in the yield, whereas the reaction did not proceed efficiently in the absence catalyst even after 10 h (Table 2). Then, the effect of temperature was studied at room temperature (25 °C), 40 °C, 60 °C and 80 °C. It was observed that the yield increased as the reaction temperature was raised. Investigation of different solvents showed the best solvent was Ethanol. The results of several experimental conditions are summarized in Table 2. As can be seen, synthesis of hydantoin and TZD derivatives using 50 mg of the catalyst Fe_3O_4@PABA-Cu(II) under reflux condition and in the presence of ethanol as a benign solvent has the best effect on the yield (98.0%).

With regards to the optimization of the reaction conditions and exploring the scope of the reaction, the present study has been extended to different kinds of a wide range of commercially available aromatic and heteroaromatic aldehydes. The results are listed in Table 3, in which the target products were afforded in moderate to excellent yields. According to the latter mentioned table, the reactions were efficiently promoted using various ortho-, meta-, and para-substituted (heterocyclic) arylaldehydes, especially

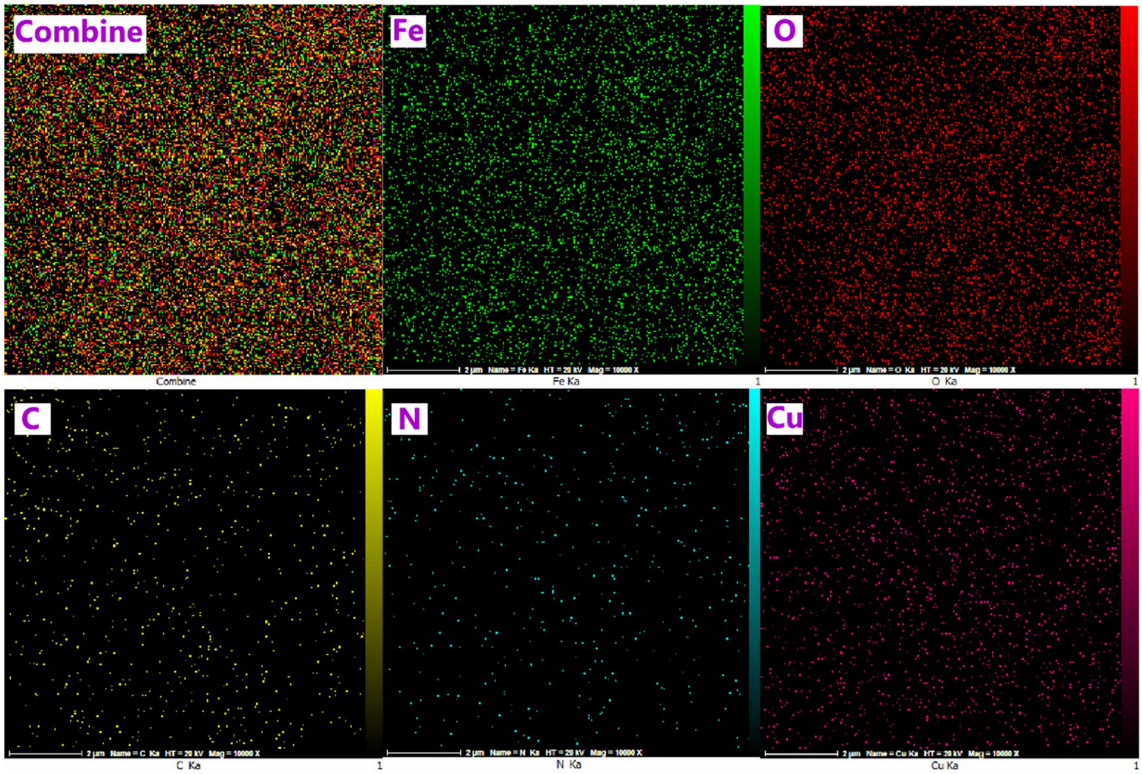

Fig. 6 EDX elemental mapping results patterns of Fe_3O_4@PABA-Cu(II)

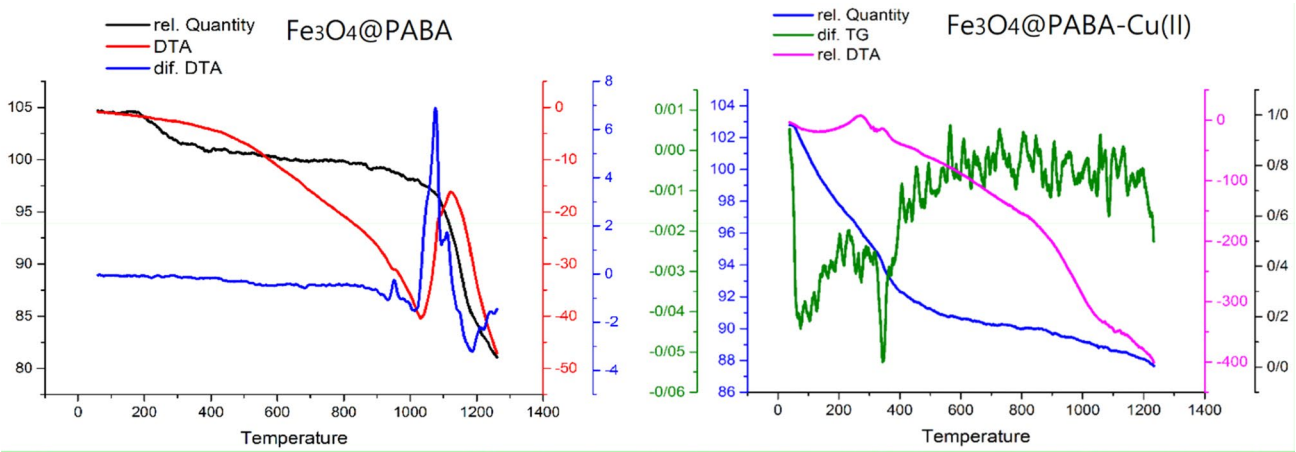

Fig. 7 TGA and differential TGA analysis spectra of **a** Fe_3O_4@PABA and **b** Fe_3O_4@PABA-Cu(II)

arylaldehydes with electron-withdrawing groups which could produce higher yields than electron-rich substitutions directly attached to the benzene or other kinds of aromatic or heteroaromatic rings. The desired pure products were characterized by comparison of their physical data (melting point, IR and ^{1}H NMR) with those of known compounds in the literature. In Table 3, it is also obvious that the (hetero) aromatic aldehydes with both kinds of electron-withdrawing or electron-releasing substituents get involved in aldol condensation in the presence of Fe_3O_4@PABA-Cu(II) to provide the corresponding product in superb efficiency and excellent yields in the reaction time ranging from 60 to 100 min. Also, fortunately, the expected products with relatively low yields could be obtained. As expected, according to our observations and the results which are summarized in Table 2, it is shown that in the presence of our newly designed Fe_3O_4@PABA-Cu(II), a wide range of (hetero) aromatic aldehydes could react with hydantoin nucleus or TZD scaffold efficiently and give 1a–10a and 1b-10b compounds in good to excellent yields (Table 3, entries 1–12) (Scheme 3).

The possible reaction pathways for the aldol condensation in the presence of Fe_3O_4@PABA-Cu(II) as a Lewis acid metal complex catalyst, is outlined in Scheme 4. Electron deficient sites on the surface of our main and final designed catalyst Fe_3O_4@PABA-Cu(II) could coordinate with the O-donor sites of hydantoin TZD and activate them for conversion to the Enol form. The electrophilicity of the carbonyl carbon atom of both aldehydes and active methylene compound (here hydantoin or TZD) increases due to coordination with the empty orbital of PABA-Cu(II) grafted at the surface of the functionalized Fe_3O_4. Subsequent aldol type condensation leads to the corresponding product [1].

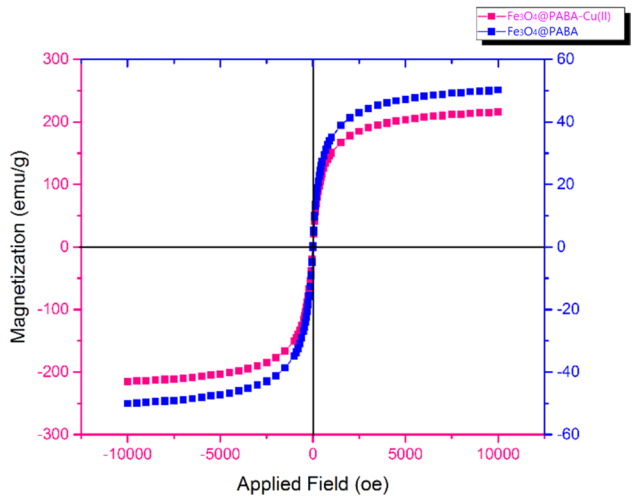

Fig. 8 The magnetic diagram of Fe_3O_4@PABA and Fe_3O_4@PABA-Cu(II)

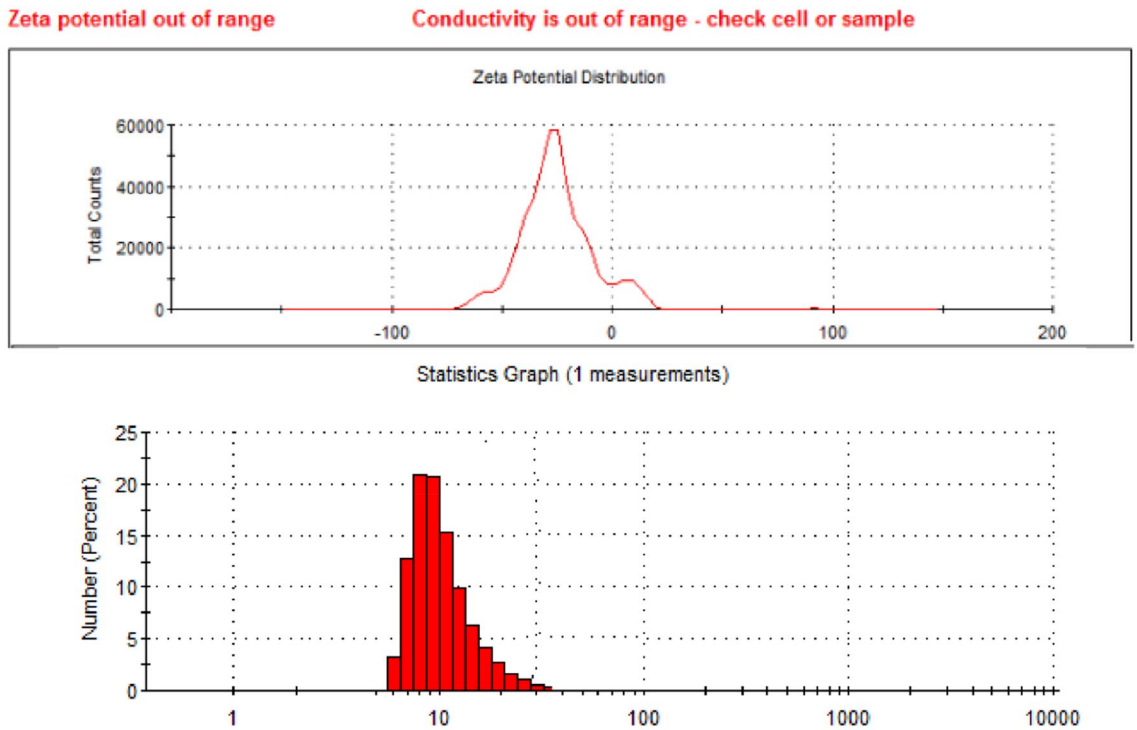

Fig. 9 Particle size distribution and zeta potential of Fe_3O_4@PABA-Cu(II) assessed by DLS

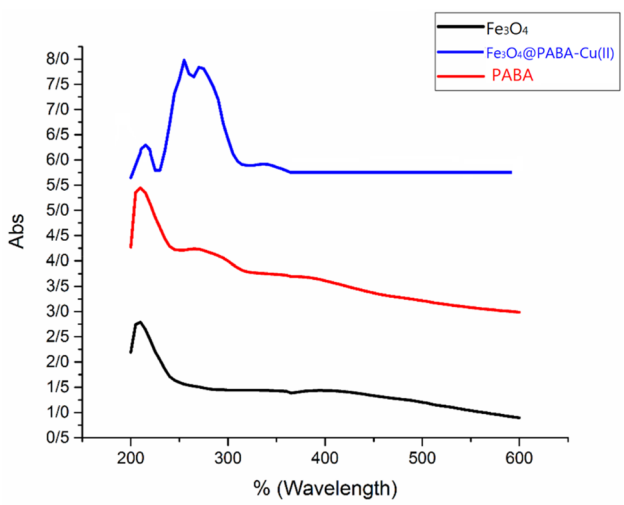

Fig. 10 UV–Vis spectroscopy of PABA, Fe_3O_4 and Fe_3O_4@PABA-Cu(II)

3.4 Recyclability Study

We investigated the recyclability of the Fe_3O_4@PABA-Cu(II) in the selected model reaction under optimized conditions, and we found that this catalyst is reusable for seven consecutive cycles. Every time after completion of the reaction as indicated by TLC (chloroform: methanol, 9:1), the reaction mixture was diluted with hot ethanol and the catalyst was easily retrieved and separated from the reaction mixture using an external magnet, washed two times with hot ethanol and acetone to completely remove organic residues from the reaction mixture and then dried at 60 °C. The recovered catalyst was reused for at most seven consecutive cycles without any significant loss in catalytic activity (Fig. 12).

After recycling the catalyst for seven runs, to show the stability and to prove the recoverability of the catalyst, we again used techniques to analyze the recovered Fe_3O_4@

Table 1 The basic optimized parameters for the determination of Cu using AAS

Wavelength (nm)	Slit (nm)	Lamp current (mA)	Lamp mode BGC	Drying (°C)	Drying time (s)	Atomization (°C)	Atomization time (s)	Cleaning (°C)	Clearing time (s)	LOD (μg kg^{-1})
324.8	0.7	8	D2	150	30	2300	5	2500	2	< 30

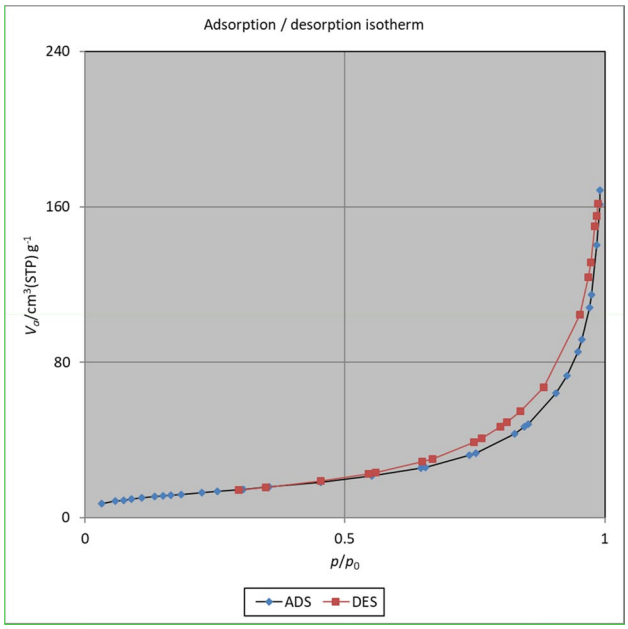

Fig. 11 The Adsorption/desorption isotherms of Fe_3O_4@PABA-Cu(II)

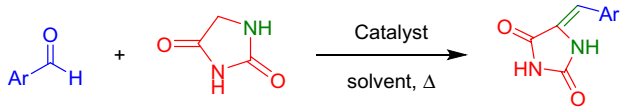

Scheme 2 Optimization of the reaction conditions in synthesis of 5-arylidenthiazolidine-2,4-diones and 5-arylidene-imidazolidine-2,4-dione derivatives

PABA-Cu(II). After spending the catalyst, the stability of recovered Fe_3O_4@PABA-Cu(II) catalyst characterized by FT-IR, SEM, EDX, XRD, VSM and TGA techniques (Fig. 13) and the results show good agreement with the fresh catalyst analysis.

3.5 Hot Filtration

The heterogeneity of Fe_3O_4@PABA-Cu(II) MNPs in the reaction mixture was studied using the hot filtration test. The hot filtration test was performed in the selected model reaction under the optimal reaction conditions. After the half reaction time, the reaction was terminated and the corresponding product was obtained in 63% of yield. Then, the reaction was repeated, and at the half time of the reaction, the catalyst was separated by magnetic separation from the reaction mixture, which was allowed to react further. Accordingly, we found that only a trace conversion (< 3%)

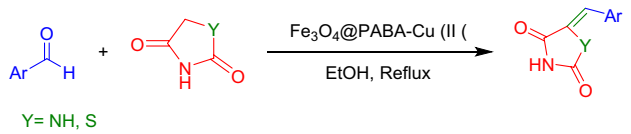

Scheme 3 Synthesis of 5-arylidenthiazolidine-2,4-diones and 5-arylidene- imidazolidine-2,4-dione derivatives in the presence of Fe_3O_4@PABA-Cu(II)

Table 2 Optimization of reaction conditions for preparing compound 10b under reflux in Ethanol

Entry	Catalyst (mg)	Temp (°C)	Solvents	Time (min)	Yield (%)[a]
1	PABA (30)	Reflux	EtOH	60	30
2	Nano- Fe_3O_4 (30)	Reflux	EtOH	60	40
3	Fe_3O_4@PABA (30)	Reflux	EtOH	60	75
4	Fe_3O_4@PABA-Cu(II) (14)	Reflux	EtOH	60	75
5	Fe_3O_4@PABA-Cu(II) (30)	Reflux	EtOH	60	75
6	Fe_3O_4@PABA-Cu(II) (50)	Reflux	EtOH	60	98
7	Fe_3O_4@PABA-Cu(II) (60)	Reflux	EtOH	60	98
8	Fe_3O_4@PABA-Cu(II) (50)	25 °C	EtOH	60	10
9	Fe_3O_4@PABA-Cu(II) (50)	40 °C	EtOH	60	20
10	Fe_3O_4@PABA-Cu(II) (50)	60 °C	EtOH	60	35
11	Fe_3O_4@PABA-Cu(II) (50)	Reflux	EtOH:H_2O (2:1)	100	78
12	Fe_3O_4@PABA-Cu(II) (50)	80 °C	H_2O	120	–
13	Fe_3O_4@PABA-Cu(II) (50)	Reflux	MeOH	120	60
14	Fe_3O_4@PABA-Cu(II) (50)	Reflux	EtOAc	180	50
15	–	Reflux	EtOH	600	Trace
16	Cu $(OAc)_2$	Reflux	EtOH	120	70

[a]The approximate isolation yields

Table 3 Preparation of 5-arylidenthiazolidine-2,4-diones and 5-arylidene- imidazolidine-2,4-dione derivatives in the presence of Fe_3O_4@PABA-Cu(II) (50 mg) as catalyst under reflux conditions in Ethanol

Entry	R	Y	Product	Time (min)	Yield (%)[a]	MP (°C) (Obs)	MP (°C) (lit)
1	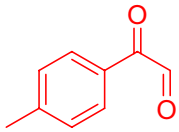	S	1a	89	97	231–232	219–220 [53]
2		NH	1b	88	98	290–294	286–287 [53]
3	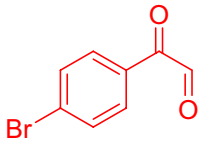	S	2a	91	95	255–256	250–252 [53]
4		NH	2b	89	97	275–277	274–275 [53]
5	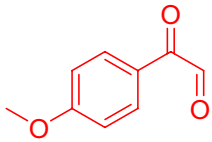	S	3a	90	98	298–299	–
6		NH	3b	89	98	288–290	213–214 [54]
7	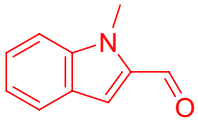	S	4a	95	95	185–186	186–187 [54]
8		NH	4b	93	96	306–307	–
9	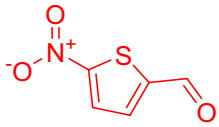	S	5a	94	96	240–242	–
10		NH	5b	93	98	214–215	–
11	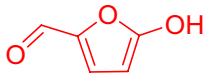	S	6a	95	94	218–220	–
12		NH	6b	94	95	182–183	–
13	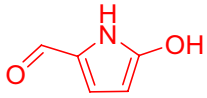	S	7a	97	90	223–224	–
14		NH	7b	95	92	219–220	–
15	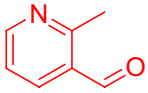	S	8a	95	94	288–290	–
16		NH	8b	94	94	295–296	–
17	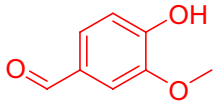	S	9a	89	94	252–253	226–226.7 [55]
18		NH	9b	88	97	270–272	249.2–251.6 [56]
19	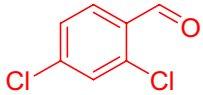	S	10a	98	95	166–167	203 [57]
20		NH	10b	97	98	188–189	257–261 [58]

Table 3 (continued)

Entry	R	Y	Product	Time (min)	Yield (%)[a]	MP (°C) (Obs)	MP (°C) (lit)
	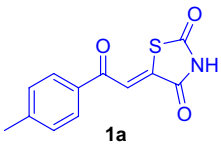	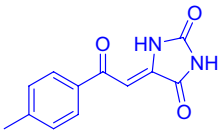	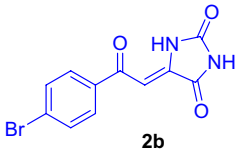				
	1a	1b	2b				
	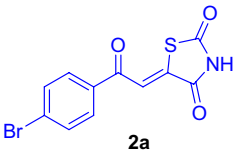	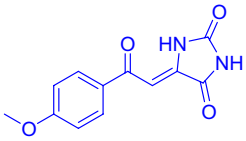	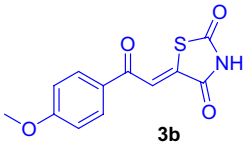				
	2a	3a	3b				
	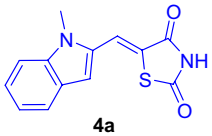	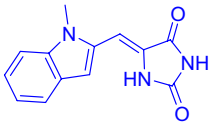	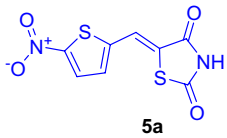				
	4a	4b	5a				
	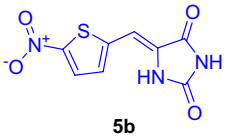	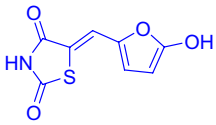	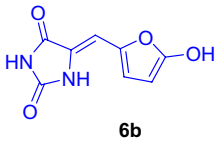				
	5b	6a	6b				
	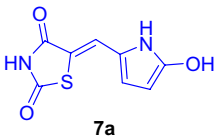	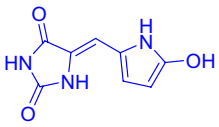	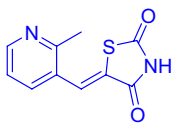				
	7a	7b	8a				
	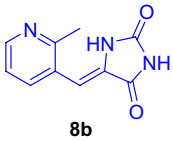	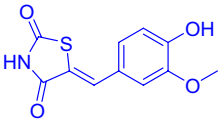	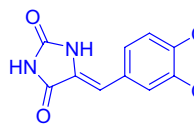				
	8b	9a	9b				
	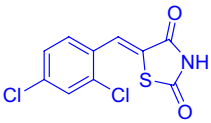	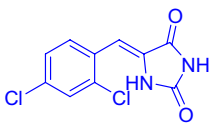					
	10a	10b					

[a]Isolated yield

of the coupling reaction was observed upon heating of the catalyst-free solution for another half time of the reaction, which means that the described nanocatalyst is completely heterogeneous in the reaction media.

3.6 Leaching Test

In order to consider the leaching of Cu into reaction media, AAS analysis was performed, the cooper content in reaction media in the selected model reaction under the optimal

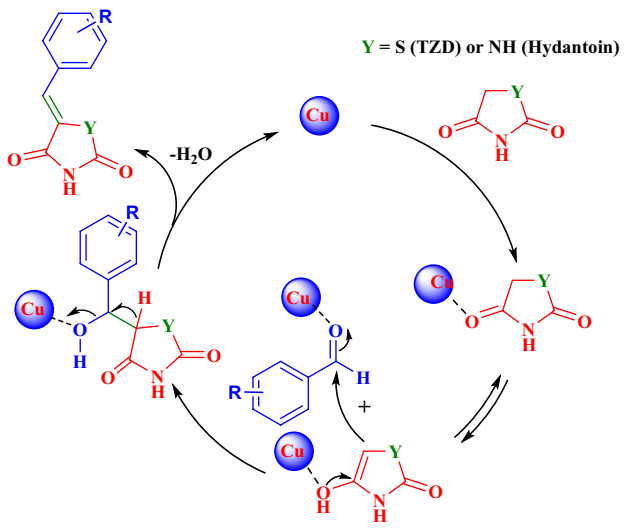

Scheme 4 Proposed mechanism for aldol condensation in the Fe_3O_4@PABA-Cu(II)

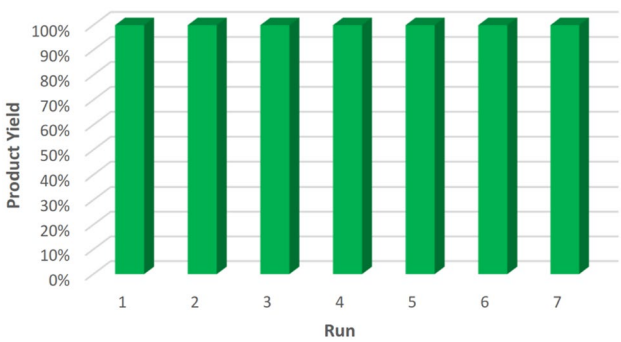

Fig. 12 Easy separation and reusability of the Fe_3O_4@PABA-Cu(II)

reaction conditions was found to be 0.81%. The results show that the leaching of Cu into reaction media is negligible.

3.7 Comparison

In order to assess the efficiency and generality of this methodology, the obtained results from the model reaction by this method have been compared with some published procedures and previously reported methods (Table 4). These results show that Fe_3O_4@PABA-Cu(II) as an efficient catalyst increase the reaction yields and rate with easy conditions, simple workup and reduced unwanted side product.

4 Conclusion

In this study, we have demonstrated a novel eco-friendly and easy approach was utilized in synthesis of the immobilized copper nanocatalyst Fe_3O_4@PABA-Cu(II). The prepared magnetic nanocatalyst characterized by using SEM, EDAX, XRD, and VSM spectroscopy. Immobilization of this simple metal catalyst on the surface of PABA modified Fe_3O_4 MNPs at its highest loading capacity, has significant advantages. This heterogeneous magnetically separable nanocatalyst can reduce the problems of using the homogenous mineral catalyst which is not recoverable. PABA as nontoxic and biocompatible compound, act as an efficient bridge between Fe_3O_4 and Cu particles to form a leak-free and stable nanocatalyst. In continuation of our previous research, this newly synthesized surface-modified MNPs as a green and reusable Nanosized catalyst was tested and exhibited excellent activity for high yield synthesis of 5-arylidenthiazolidine-2,4-diones and 5-arylidene-imidazolidine-2,4-dione derivatives through condensation reaction between (hetero)aromatic aldehydes and hydantoin or TZD main cores, under reflux conditions in Ethanol as a benign and green solvent. This economical protocol and green methodology of this study show clear advantages over traditional catalytic methods that include avoidance of hazardous organic solvents, recoverability of the catalyst, lower formation of the byproducts and less toxicity, high percentage yield, short reaction time and easy workup by a simple external magnet after completion of the reaction. Therefore, coating MNPs with PABA as a bridge and structural scaffold for immobilizing the copper(II) complex on the PABA coated Fe_3O_4 MNPs, may find extensive applications especially in aldol condensation reaction reactions. Furthermore, according to our results, the intermediate agent MNPs-PABA also display considerable catalytic activity in aldolization.

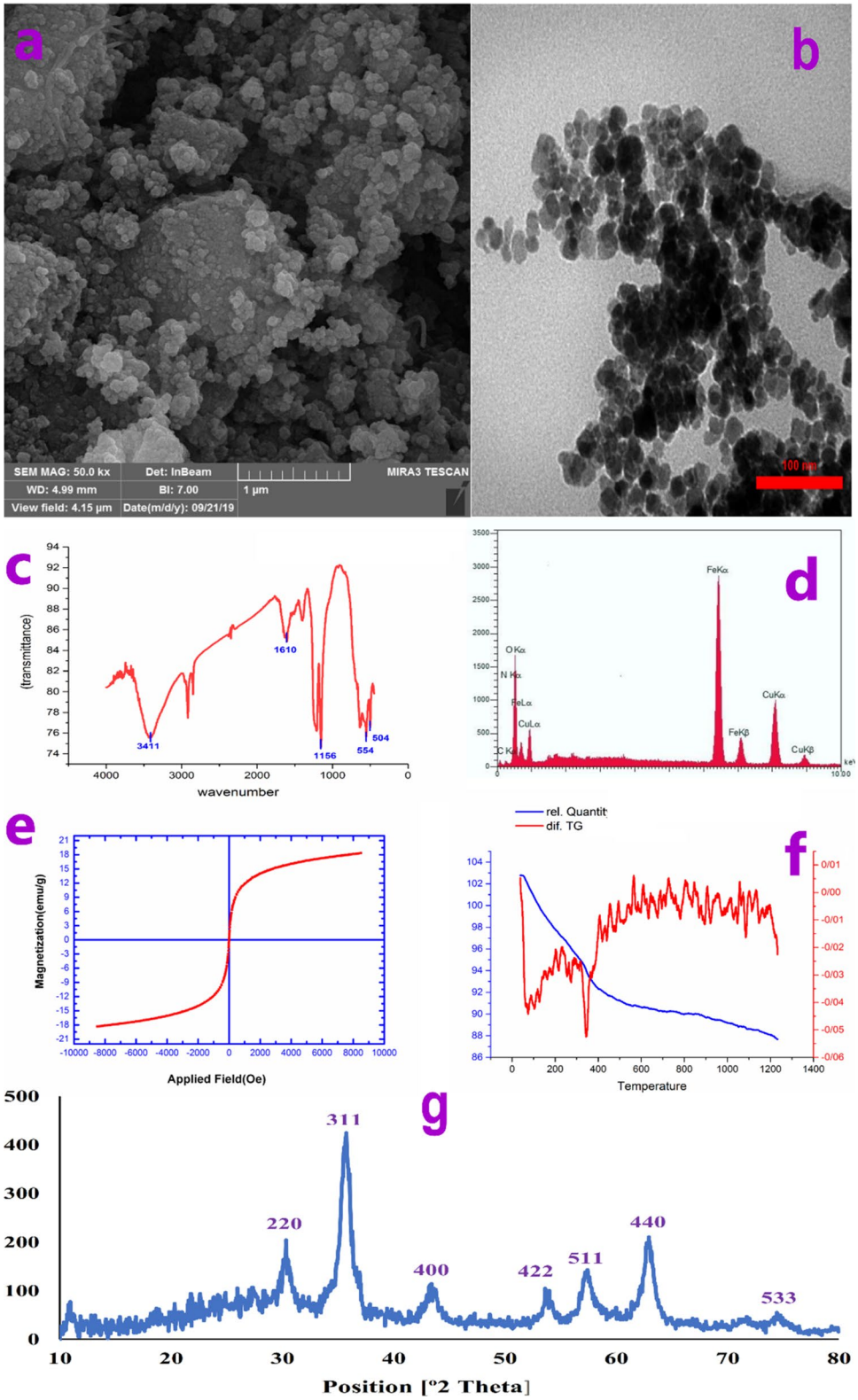

Fig. 13 **a** SEM, **b** TEM, **c** FT-IR, **d** EDAX, **e** VSM, **f** TGA and differential TGA and **g** XRD analysis of the recovered Fe_3O_4@PABA-Cu(II)

Table 4 Comparison of the efficiency of Fe_3O_4@PABA-Cu(II) with other reported catalysts in literature condensation

Entry	Catalyst/conditions	Time (Min)	Yield (%)[a]	Ref.
1	2-HEAP/solvent-free conditions	180	72	[59]
2	Alum/microwave	10–60	55	[60]
3	Base/solvent	360–780	50	[61]
4	$BiCl_3$/microwave	240–480	85	[62]
5	piperidine, HOAc/microwave	90	50	[63]
6	Fe_3O_4@PABA-Cu(II)/ethanol, reflux	60	98	This work

[a]Isolated yield

References

1. Akhavan M, Foroughifar N, Pasdar H et al (2017) Copper(II)-complex functionalized magnetite nanoparticles: a highly efficient heterogeneous nanocatalyst for the synthesis of 5-arylidenthiazolidine-2,4-diones and 5-arylidene-2-thioxothiazolidin-4-one. Transit Met Chem 42:543–552. https://doi.org/10.1007/s11243-017-0159-3
2. Pu Q, Kazemi M, Mohammadi M (2019) Application of transition metals in sulfoxidation reactions. Mini Rev Org Chem 16:5775–5791. https://doi.org/10.2174/1570193X16666190430154835
3. Chen L, Noory Fajer A, Yessimbekov Z et al (2019) Diaryl sulfides synthesis: copper catalysts in C–S bond formation. J Sulfur Chem 40:451–468. https://doi.org/10.1080/17415993.2019.1596268
4. Ghorbani-Choghamarani A, Mohammadi M, Tamoradi T, Ghadermazi M (2019) Covalent immobilization of Co complex on the surface of SBA-15: Green, novel and efficient catalyst for the oxidation of sulfides and synthesis of polyhydroquinoline derivatives in green condition. Polyhedron 158:25–35. https://doi.org/10.1016/j.poly.2018.10.054
5. Filian H, Kohzadian A, Mohammadi M et al (2020) Pd(0)-guanidine@MCM-41: a very effective catalyst for rapid production of bis (pyrazolyl)methanes. Appl Organomet Chem. https://doi.org/10.1002/aoc.5579 **(Article in press)**
6. Ghorbani-Choghamarani A, Mohammadi M, Hudson RHE, Tamoradi T (2019) Boehmite@tryptophan-Pd nanoparticles: a new catalyst for C-C bond formation. Appl Organomet Chem 33:e4977. https://doi.org/10.1002/aoc.4977
7. Kazemi M, Mohammadi M (2020) Magnetically recoverable catalysts: catalysis in synthesis of polyhydroquinolines. Appl Organomet Chem 34:e5400. https://doi.org/10.1002/aoc.5400
8. Ghorbani-Choghamarani A, Mohammadi M, Shiri L, Taherinia Z (2019) Synthesis and characterization of spinel $FeAl_2O_4$ (hercynite) magnetic nanoparticles and their application in multicomponent reactions. Res Chem Intermed 45:5705–5723. https://doi.org/10.1007/s11164-019-03930-0
9. Ghorbani-Choghamarani A, Mohammadi M, Taherinia Z (2019) (ZrO)2Fe2O5 as an efficient and recoverable nanocatalyst in C–C bond formation. J Iran Chem Soc 16:411–421. https://doi.org/10.1007/s13738-018-1522-9
10. Nikoorazm M, Khanmoradi M, Mohammadi M (2020) Guanine-La complex supported onto SBA-15: a novel efficient heterogeneous mesoporous nanocatalyst for one-pot, multi-component Tandem Knoevenagel condensation–Michael addition–cyclization reactions. Appl Organomet Chem. https://doi.org/10.1002/aoc.5504
11. Mahmoudi-GomYek S, Azarifar D, Ghaemi M et al (2019) Fe_3O_4-supported Schiff-base copper (II) complex: a valuable heterogeneous nanocatalyst for one-pot synthesis of new pyrano[2,3-b]pyridine-3-carboxamide derivatives. Appl Organomet Chem 33:e4918. https://doi.org/10.1002/aoc.4918
12. Rofouei MK, Aghaei A (2013) Synthesis and spectroscopic studies of some new ortho functionalized triazene compounds and their reactivity with mercury (II) ion. J Iran Chem Soc 10:969–977. https://doi.org/10.1007/s13738-013-0234-4
13. Tamoradi T, Mousavi SM, Mohammadi M (2020) Praseodymium(iii) anchored on $CoFe_2O_4$ MNPs: an efficient heterogeneous magnetic nanocatalyst for one-pot, multi-component domino synthesis of polyhydroquinoline and 2,3-dihydroquinazolin-4(1H)-one derivatives. New J Chem 44:3012–3020. https://doi.org/10.1039/C9NJ05468E
14. Kazemi M, Ghobadi M, Mirzaie A (2018) Cobalt ferrite nanoparticles (CoFe2O4 MNPs) as catalyst and support: magnetically recoverable nanocatalysts in organic synthesis. Nanotechnol Rev 7:43–68. https://doi.org/10.1515/ntrev-2017-0138
15. Mohammadi M, Ghorbani-Choghamarani A (2020) L-Methionine–Pd complex supported on hercynite as a highly efficient and reusable nanocatalyst for C–C cross-coupling reactions. New J Chem 44:2919–2929. https://doi.org/10.1039/C9NJ05325E
16. Kazemi M, Nasr SM, Chen Z, Mohammadi M (2019) A mini-review: achievements in the thiolysis of epoxides. Mini Rev Org Chem 16:1–11. https://doi.org/10.2174/1570193x16666190723111746
17. Kolvari E, Koukabi N, Khoramabadi-zad A et al (2014) Alternative methodologies for halogenation of organic compounds. Curr Org Synth 10:837–863. https://doi.org/10.2174/1570179410061402061025 41
18. Da OhW, Lim TT (2019) Design and application of heterogeneous catalysts as peroxydisulfate activator for organics removal: an overview. Chem Eng J 358:110–133. https://doi.org/10.1016/j.cej.2018.09.203
19. Trimm DL, Stanislaus A (1986) The control of pore size in alumina catalyst supports: a review. Appl Catal 21:215–238. https://doi.org/10.1016/S0166-9834(00)81356-1
20. Lima CGS, Jorge EYC, Batinga LGS et al (2019) ZSM-5 zeolite as a promising catalyst for the preparation and upgrading of lignocellulosic biomass-derived chemicals. Curr Opin Green Sustain Chem 15:13–19. https://doi.org/10.1016/j.cogsc.2018.08.001
21. Chen MN, Mo LP, Cui ZS, Zhang ZH (2019) Magnetic nanocatalysts: synthesis and application in multicomponent reactions. Curr Opin Green Sustain Chem 15:27–37. https://doi.org/10.1016/j.cogsc.2018.08.009
22. Heravi M, Faghihi Z (2014) Applications of heteropoly acids in multi-component reactions. J Iran Chem Soc 11:209–224. https://doi.org/10.1007/s13738-013-0291-8
23. Lashanizadegan M, Zareian Z (2011) Homogenous and heterogeneous catalytic activity of Azo-linked Schiff base complexes of Mn(II), Cu(II) and Co(II). Catal Lett 141:1698–1702. https://doi.org/10.1007/s10562-011-0709-9
24. Afradi M, Pour SA, Dolat M, Yazdani-Elah-Abadi A (2018) Nanomagnetically modified vitamin B3 (Fe_3O_4@Niacin): an efficient and reusable green biocatalyst for microwave-assisted rapid

synthesis of 2-amino-3-cyanopyridines in aqueous medium. Appl Organomet Chem 32:e4103. https://doi.org/10.1002/aoc.4103
25. Rezapour E, Jafarpour M, Rezaeifard A (2018) Palladium niacin complex immobilized on starch-coated maghemite nanoparticles as an efficient homo- and cross-coupling catalyst for the synthesis of symmetrical and unsymmetrical biaryls. Catal Lett 148:3165–3177. https://doi.org/10.1007/s10562-018-2513-2
26. Maleki M, Baghbanian SM, Tajbakhsh M (2018) Heteropolyacid immobilized on polymer/magnetic zeolite nanocomposite as a new and recyclable catalyst for the selective oxidation of alcohols. J Iran Chem Soc 15:359–368. https://doi.org/10.1007/s13738-017-1237-3
27. Maleki A, Jafari AA, Yousefi S (2017) $MgFe_2O_4$/cellulose/SO3H nanocomposite: a new biopolymer-based nanocatalyst for one-pot multicomponent syntheses of polysubstituted tetrahydropyridines and dihydropyrimidinones. J Iran Chem Soc 14:1801–1813. https://doi.org/10.1007/s13738-017-1120-2
28. Veisi H, Mohammadi L, Hemmati S et al (2019) In situ immobilized silver nanoparticles on *Rubia tinctorum* extract-coated ultrasmall iron oxide nanoparticles: an efficient nanocatalyst with magnetic recyclability for synthesis of propargylamines by A3 coupling reaction. ACS Omega 4:13991–14003. https://doi.org/10.1021/acsomega.9b01720
29. Zolfigol MA, Ayazi-Nasrabadi R (2016) Synthesis of the first magnetic nanoparticles with a thiourea dioxide-based sulfonic acid tag: application in the one-pot synthesis of 1,1,3-tri(1:H-indol-3-yl) alkanes under mild and green conditions. RSC Adv 6:69595–69604. https://doi.org/10.1039/c6ra11620e
30. Vernoux P, Lizarraga L, Tsampas MN et al (2013) Ionically conducting ceramics as active catalyst supports. Chem Rev 113:8192–8260. https://doi.org/10.1021/cr4000336
31. Amouri H, Desmarets C, Moussa J (2012) Confined nanospaces in metallocages: guest molecules, weakly encapsulated anions, and catalyst sequestration. Chem Rev 112:2015–2041. https://doi.org/10.1021/cr200345v
32. Marson CM (2012) Multicomponent and sequential organocatalytic reactions: diversity with atom-economy and enantiocontrol. Chem Soc Rev 41:7712–7722. https://doi.org/10.1039/c2cs35183h
33. Sun C, Zhou R, Jianan E et al (2016) Ascorbic acid-coated Fe_3O_4 nanoparticles as a novel heterogeneous catalyst of persulfate for improving the degradation of 2,4-dichlorophenol. RSC Adv 6:10633–10640. https://doi.org/10.1039/c5ra22491h
34. Vessally E, Hosseinian A, Edjlali L et al (2016) New route to 1,4-oxazepane and 1,4-diazepane derivatives: synthesis from: N-propargylamines. RSC Adv 6:99781–99793. https://doi.org/10.1039/c6ra20718a
35. Azarifar D, Tadayoni M, Ghaemi M (2018) γ-Fe_2O_3@Cu_3Al-LDH-TUD as a new amphoteric, highly efficient and recyclable heterogeneous catalyst for the solvent-free synthesis of dihydropyrano[3,2-c]pyrazoles and dihydropyrano[3,2-c]chromens. Appl Organomet Chem. https://doi.org/10.1002/aoc.4293
36. Min X, Yang W, Hui YF et al (2017) Fe_3O_4@ZIF-8: a magnetic nanocomposite for highly efficient UO^{22+} adsorption and selective UO^{22+}/Ln^{3+} separation. Chem Commun 53:4199–4202. https://doi.org/10.1039/c6cc10274c
37. Sepehrmansouri H, Zarei M, Zolfigol MA et al (2019) Multilinker phosphorous acid anchored En/MIL-100(Cr) as a novel nanoporous catalyst for the synthesis of new N-heterocyclic pyrimido[4,5-b]quinolines. Mol Catal 481:110303
38. Rezaei M, Azizi K, Amani K (2018) Copper–birhodanine complex immobilized on Fe_3O_4 nanoparticles: DFT studies and heterogeneous catalytic applications in the synthesis of propargylamines in aqueous medium. Appl Organomet Chem. https://doi.org/10.1002/aoc.4120
39. Dehbanipour Z, Moghadam M, Tangestaninejad S et al (2017) Copper(II) bis-thiazole complex immobilized on silica nanoparticles: preparation, characterization and its application as a highly efficient catalyst for click synthesis of 1,2,3-triazoles. Polyhedron 138:21–30. https://doi.org/10.1016/j.poly.2017.08.032
40. Khodaei MM, Bahrami K, Meibodi FS (2017) Ferromagnetic nanoparticle-supported copper complex: a highly efficient and reusable catalyst for three-component syntheses of 1,4-disubstituted 1,2,3-triazoles and C-S coupling of aryl halides. Appl Organomet Chem 31:e3714. https://doi.org/10.1002/aoc.3714
41. Xu Z, Hou Y, Sun S (2007) Magnetic core/shell Fe_3O_4/Au and Fe_3O_4/Au/Ag nanoparticles with tunable plasmonic properties. J Am Chem Soc 129:8698–8699. https://doi.org/10.1021/ja073057v
42. Kumar BRP, Nanjan MJ (2010) Novel glitazones: design, synthesis, glucose uptake and structure-activity relationships. Bioorg Med Chem Lett 20:1953–1956. https://doi.org/10.1016/j.bmcl.2010.01.125
43. Sandhu JS (2013) Ultrasound-assisted synthesis of 2,4-thiazolidinedione and rhodanine derivatives catalyzed by task-specific ionic liquid: [TMG][Lac]. Org Med Chem Lett 3:2. https://doi.org/10.1186/2191-2858-3-2
44. Khajeh-Amiri A, Foroughifar N, Hassannejad F et al (2019) Microwave assisted highly efficient synthesis of rhodanine and -2, 4-thiazolidinedione derivatives under solvent free conditions. Curr Microw Chem 06:215–224. https://doi.org/10.2174/2213335606666190118163108
45. Jawale DV, Pratap UR, Lingampalle DL, Mane RA (2011) Dicationic ionic liquid mediated synthesis of 5-arylidine-2,4-thiazolidinediones. Chin J Chem 29:942–946. https://doi.org/10.1002/cjoc.201190192
46. Kumar KK, Sharma RSK, Babu PC et al (2017) Synthesis, characterization and pharmacological evaluation of novel spiro heterocyclic compounds as anti diabetic agents. Asian J Res Chem 10:393. https://doi.org/10.5958/0974-4150.2017.00067.0
47. Nikalje A, Nikalje G, Deshpande D, Une H (2012) Facile synthesis and in vivo hypoglycemic activity of novel 2,4-hiazolidinedione derivatives. Eur J Exp Biol 2:343–353
48. Ceylan-Ünlüsoy M, Verspohl EJ, Ertan R (2010) Synthesis and antidiabetic activity of some new chromonyl-2,4-thiazolidinediones. J Enzyme Inhib Med Chem 25:784–789. https://doi.org/10.3109/14756360903357544
49. Marbois B, Xie LX, Choi S et al (2010) para-aminobenzoic acid is a precursor in coenzyme Q6 biosynthesis in *Saccharomyces cerevisiae*. J Biol Chem 285:27827–27838. https://doi.org/10.1074/jbc.M110.151894
50. Riedlinger J, Reicke A, Zähner H et al (2004) Abyssomicins, inhibitors of the para-aminobenzoic acid pathway produced by the marine Verrucosispora strain AB-18-032. J Antibiot 57:271–279. https://doi.org/10.7164/antibiotics.57.271
51. Ashraf MA, Liu Z, Peng W-X, Gao C (2020) New copper complex on Fe_3O_4 nanoparticles as a highly efficient reusable nanocatalyst for synthesis of polyhydroquinolines in water. Catal Lett 150:683–701. https://doi.org/10.1007/s10562-019-02986-2
52. Gasparro FP (1985) UV-induced photoproducts of paraaminobenzoid acid. Photodermatology 2:151–157
53. Omar MT, Fouli AE, El-Garhi MZ (1991) Studies on 4-thiazolidinones. IX. The conversion of 5-substituted 2-thioxo-4-thiazolidinones into corresponding 2,4-thiazolidinones. Bull Chem Soc Jpn 64:750–752. https://doi.org/10.1246/bcsj.64.750
54. Zalesov VS, Andreichikov YS, Nalimova YA et al (1978) Chemistry of oxalyl derivatives of methyl ketones: XIX. Synthesis and biological activity of 5-phenacylidenyl-tetrahydroimidazole-2,4-diones. Pharm Chem J 12:906–909. https://doi.org/10.1007/BF00777636
55. Jahanshahi R, Akhlaghinia B (2016) CuII immobilized on guanidinated epibromohydrin functionalized γ-Fe_2O_3@TiO_2 (γ-Fe_2O_3@

TiO_2-EGCuII): a novel magnetically recyclable heterogeneous nanocatalyst for the green one-pot synthesis of 1,4-disubstituted 1,2,3-triazoles through alkyne-azide cycload. RSC Adv 6:29210–29219. https://doi.org/10.1039/c6ra05468d
56. Ha YM, Kim JA, Park YJ et al (2011) Analogs of 5-(substituted benzylidene)hydantoin as inhibitors of tyrosinase and melanin formation. Biochim Biophys Acta 1810:612–619. https://doi.org/10.1016/j.bbagen.2011.03.001
57. Leite FHA, da Silva Santiago PBG, Froes TQ et al (2016) Structure-guided discovery of thiazolidine-2,4-dione derivatives as a novel class of Leishmania major pteridine reductase 1 inhibitors. Eur J Med Chem 123:639–648. https://doi.org/10.1016/j.ejmech.2016.07.060
58. Thenmozhiyal JC, Wong PTH, Chui WK (2004) Anticonvulsant activity of phenylmethylenehydantoins: a structure-activity relationship study. J Med Chem 47:1527–1535. https://doi.org/10.1021/jm030450c
59. Kang TH, Matsumoto K, Tohda M et al (2002) Pteropodine and isopteropodine positively modulate the function of rat muscarinic M1 and 5-HT2 receptors expressed in *Xenopus oocyte*. Eur J Pharmacol 444:39–45. https://doi.org/10.1016/S0014-2999(02)01608-4
60. Shelke KF, Sapkal SB, Kakade GK et al (2010) Alum catalyzed simple and efficient synthesis of 5-arylidene-2,4-thiazolidinedione in aqueous media. Green Chem Lett Rev 3:17–21. https://doi.org/10.1080/17518250903478345
61. Mahalle S, Ligampalle D, Mane R (2009) Microwave-assisted synthesis of some 2,4-thiazolidinedione derivatives. Heteroat Chem An Int J Main Gr Elem 20:151–156
62. Shah S, Singh B (2012) Urea/thiourea catalyzed, solvent-free synthesis of 5-arylidenethiazolidine-2,4-diones and 5-arylidene-2-thioxothiazolidin-4-ones. Bioorg Med Chem Lett 22:5388–5391
63. Drawanz BB, Ribeiro CS, Masteloto HG et al (2014) Sonochemistry: a good, fast and clean method to promote the synthesis of 5-arylidene-2,4-thiazolidinediones. Ultrason Sonochem 21:1615–1617. https://doi.org/10.1016/j.ultsonch.2014.04.013

Affiliations

Zohreh Esam[1,2] · Malihe Akhavan[1] · Ahmadreza Bekhradnia[1,3] · Masoud Mohammadi[4] · Saeed Tourani[1]

Ahmadreza Bekhradnia
reza_bnia@yahoo.com

[1] Department of Medicinal Chemistry, Faculty of Pharmacy, Mazandaran University of Medical Sciences, Sari, Iran

[2] Department of Medicinal Chemistry, Faculty of Pharmacy, Ayatollah Amoli Branch, Islamic Azad University, Amol, Iran

[3] Department of Chemistry and Biochemistry, Montana State University, 103CBB, Bozeman, MT 59717, USA

[4] Department of Chemistry, Faculty of Science, Ilam University, P.O. Box 69315516, Ilam, Iran